Asteroid Interiors

Erik Asphaug
University of California, Santa Cruz

Eileen V. Ryan
New Mexico Highlands University

Maria T. Zuber
Massachusetts Institute of Technology

Asteroids represent a geophysical frontier of considerable scientific importance, for these building blocks of planets preserve a compositional and mechanical record of the solar system's origin. They also pose a formidable hazard to life on Earth, while offering potentially enormous resources to benefit solar system exploration. This chapter introduces their geologic subtlety through the theme of strength vs. gravity: Asteroids stand apart from rocks and planets because these primary forces (strength short-range and gravity long-range) achieve an intricate mechanical balance that is only partly understood. Recent findings have turned Earth-based intuition on its head. For example, structurally weak asteroids and comets may, through stress dissipation, be the most highly resistant to catastrophic disruption. Perhaps more surprising, the collisional evolution of bodies the size of a city block may be determined by their minuscule self-gravity. While the fundamental geophysical behavior of asteroids continues to elude us, one idea resonates: Instead of competing for dominance, strength and gravity collaborate over a wide spectrum of sizes and shapes to produce some of the richest structures in nature.

1. INTRODUCTION

The gravity of a small asteroid can barely hold on to its rocks, yet the best spacecraft images of ~10-km bodies show fields of boulders, lunarlike craters with dramatic rim deposits, landscapes mantled in mature regolith, and shapes broadly conforming to gravity potentials (see *Sullivan et al.,* 2002). But gravity's influence must decrease with decreasing mass, and asteroids smaller than some diameter are governed by strength. But how small? Smaller than tiny Dactyl? This ~1-km satellite of Ida [the first confirmed asteroid satellite, imaged by *Galileo* en route to Jupiter (*Belton et al.,* 1996)] is a spheroid possessing what appear to be central peak craters. These characteristics indicate gravitational control, yet anything traveling faster than a half meter per second will escape Dactyl's surface. [For a nonrotating asteroid with bulk density $\rho \sim 2$ g cm^{-3}, escape velocity (in meters per second) is about equal to asteroid radius (in kilometers). If you can jump half a meter on Earth, you can leap off a 5-km-diameter asteroid.] Smaller than near-Earth asteroid Castalia? The first imaged asteroid (*Ostro et al.,* 1990), Castalia is believed to consist of two ~800-m lobes resting against one another self-gravitationally. Detailed examination of even smaller objects has just begun (see *Pravec et al.,* 2002; and *Ostro et al.,* 2002), but for reasons we shall see, gravity may control the evolution of asteroids the size of a city block, whose escape velocities are much slower than a page turning.

This is at serious odds with Earth-based intuition. Indeed, most early ideas about asteroids have proven wrong. The recent adoption of modern geophysical ideas (rate- and size-dependent strength, micro- and macroporosity), together with laboratory, numerical, and dynamical advances described below, have led to the overturn of several fundamental concepts regarding asteroid geodynamics and mechanics. Their behavior is certainly not trivial, and it is appropriate to say that the study of asteroids expands our geophysical experience to include low-gravity test beds of processes that remain poorly understood on Earth. Granular flow, impact cratering mechanics, studies of wave attenuation and fault motion in geologic media, and the mechanics of landslides may all be advanced considerably by studying the geophysics of asteroids. Of course, they also deserve our scrutiny for pragmatic reasons. The common kilometer-sized asteroids most hazardous to life on Earth might exist in a no-man's land where neither gravity nor strength predominates, and may be stranger than ever imagined.

2. STRENGTH AND GRAVITY

To understand the collisional evolution of asteroids and comets, researchers in the 1960s began using laboratory

impact experiments to determine relations between initial conditions (e.g., speed and angle of impact, structure and composition of target) and outcome (e.g., kinetic energy required for breakup, velocity and rotation of fragments). This database (see *Fujiwara et al.,* 1989; *Martelli et al.,* 1994; *Holsapple et al.,* 2002) guides our understanding of impact physics, although the experiments are limited to small projectiles whose masses can be accelerated to speeds (several kilometers per second) typical of asteroid collisions. The largest laboratory targets are orders of magnitude smaller than any asteroid; Earth's gravity overwhelms self-gravity, to be sure, and also overwhelms delicate strength effects that may be important at large scale. Chemical and nuclear explosions (*Rodionov et al.,* 1972; *Perret et al.,* 1967) provide an analogous experimental database at geologic scales, although an explosion in a half-space is significantly different from impact into a finite, irregular target. Despite these limitations, laboratory-scale impacts and high-yield explosions constitute important benchmarks against which asteroid collisional models must be gauged. But as we shall see, the best benchmarks are the cratered asteroids themselves.

It has long been recognized (*Gault et al.,* 1972; *Fujiwara,* 1980) that impact disruption depends upon target size, so two approaches were taken to extrapolate laboratory data to relevant scales. Hydrodynamical similarity ["scaling" (see *Holsapple et al.,* 2002, and references therein)] is a powerful approach that offers a unique ability to provide meaningful relationships between key parameters, for instance, fragment size as a function of impact energy and momentum, or ejecta velocity as a function of rock strength. The most significant limitation of scaling is that it presumes a homogeneous continuum, i.e., bodies that are either monolithic or finely comminuted. Where competing length scales exist (e.g., size of projectile comparable to or smaller than size of structural components in an aggregate, or crater diameter comparable to target diameter) or where target structure and shape is important (contact binary or coarsely shattered asteroids), the technique may break down. But for well-posed problems (notably half-space cratering into homogeneous media) the technique has a well-established utility. Scaling also has the distinct advantages of providing direct physical intuition (for instance, how crater diameter relates to impact speed) and requiring no major computational effort.

A very different approach is to directly integrate the shock physics relations, together with an equation of state plus the mass, momentum, and energy conservation equations of continuum mechanics. These "hydrocodes" are versatile and on modern computers can be run with adequate resolution and fidelity to model targets with layers, cores, realistic shapes, prefractures, and multiple components. [The term "hydrocode" broadly describes any explicit continuum mechanics code capable of modeling shock physics and the behavior of solid media under high dynamic stress. Originally applied only to extreme conditions where rock strength can be ignored ("hydro"), these codes have evolved to model distinctively nonfluid behaviors such as elasticity and fragmentation.] But hydrocodes are seldom easy to use and the data they produce are not trivial to interpret. As with all tools, hydrocodes are easier to misuse than use. One common culprit is lack of resolution adequate to resolve the impact shock. The shock determines the velocities in the excavation flow, and hence the growth of a gravity-regime crater, or disassembly following catastrophic disruption. Other errors include the use of an inappropriate equation of state, application of a model beyond its designed domain, and misinterpretation of results. Furthermore, although these numerical techniques date back half a century (e.g., *von Neumann and Richtmyer,* 1950), hydrocode modeling is considered by many to be an immature technique. Fortunately, hydrocode outcomes can be tested in detail against laboratory experiments for cratering and catastrophic disruption (*Melosh et al.*, 1992; *Benz and Asphaug,* 1994, 1995; *Ryan and Melosh,* 1998). Thus verified, a code can be applied with some confidence to more complex scenarios and much larger sizes that are typical of asteroids.

While there remains some conflict between scaling vs. numerical modeling (particularly in the half-space cratering regime), the predictions for catastrophic disruption appear to have achieved some convergence, encouraging us to apply laboratory-validated code models to the fundamental issues of gravity, strength, and structure on asteroids. Furthermore, if asteroids are complicated entities with odd shapes, rotations, prefractures, and porosities, numerical approaches may be the only way, short of *in situ* experiments, of understanding their behavior.

2.1. Strong Asteroids

Two decades ago it was widely believed on the basis of scaling from impact experiments (*Gault and Heitowit,* 1963; *Housen et al.,* 1979) that rocky asteroids smaller than ~70 km diameter and icy bodies smaller than ~20 km would lack regolith (cf. *Veverka et al.,* 1986). [Correcting for a typesetting error: A line was skipped on p. 354 of *Satellites*, so that it would appear that the 20-km limit applied to rock, not ice (K. Housen, personal communication, 2001).] Smaller bodies could not hold onto loose material because their craters would form in the strength regime, with nearly all material being accelerated to speeds $>v_{esc}$. [The two classical regimes of impact cratering are the strength regime and the gravity regime. Other regimes can also be defined (see *Housen et al.,* 1983), depending on the dominant force restricting crater growth. Craters forming in the strength regime must break apart rock, in which case the energy of fragmentation (the rock strength) is proportional to the energy of ejection. For craters forming in the gravity regime, ejection velocity scales with v_{esc}.] Nor could asteroids smaller than this size retain primordial regolith, because scaled experiments showed that any surface debris would rapidly erode by impacts down to bedrock. Because regolith is a common component of meteorites (see *Bunch and Rajan,* 1988), regolith breccias were believed to derive

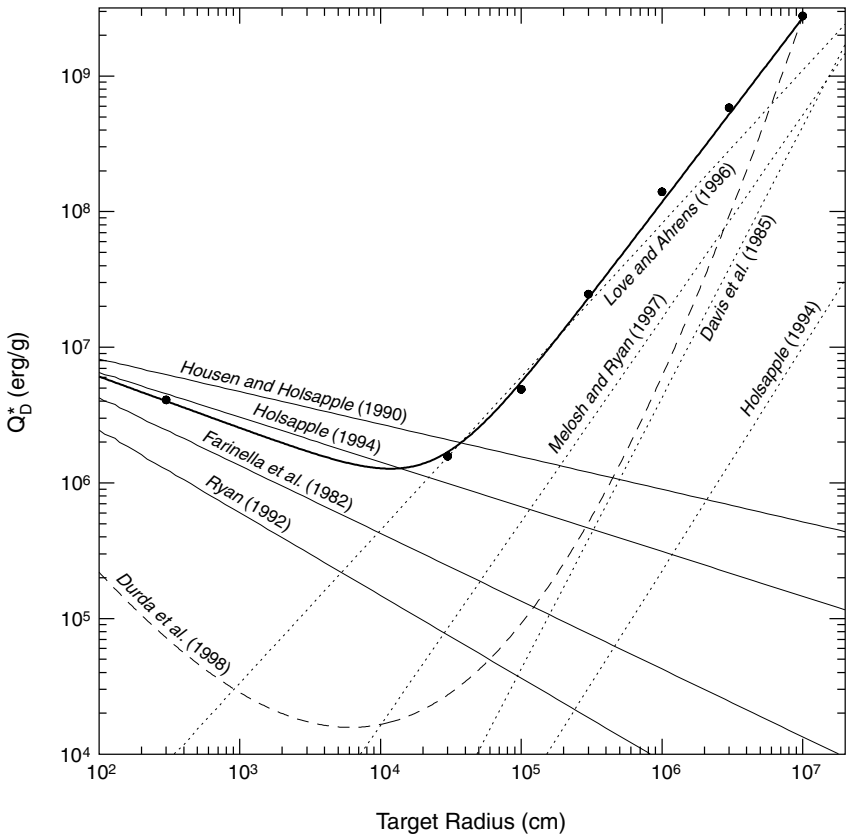

Fig. 1. Values for the catastrophic disruption threshold Q^*_D of asteroids vary widely in the literature. The darker line is the summary of numerical outcomes for basalt spheres by *Benz and Asphaug* (1999). The general trend for all models is that rocks get weaker with size because of size- and/or rate-dependent strength, and then get stronger once self-gravity dominates. For a collisionally evolved population, objects to the right of the minimum (the strength-gravity transition) are likely to be shattered but not dispersed.

from parent bodies hundreds of kilometers across, or from primordial surfaces prior to the onset of erosive collisions (*Chapman,* 1976).

A related early puzzle concerned asteroid families, whose members have orbital elements suggestive of dispersal by catastrophic impact (*Hirayama,* 1923) at speeds of hundreds of meters per second (*Cellino et al.,* 1999). For these family members to have survived such dramatic impact acceleration, it seemed that their parent rock must have been strong [see *Chapman et al.* (1989) for a variety of asteroid family hypotheses]. Strong targets would yield fast, large family members whose strength might thereafter resist catastrophic disruption over the billions of years to the present day. The argument for strong asteroids was not entirely satisfying to those who have seen primitive meteorites fall apart in their hands, but it was largely self-consistent. [High ejection speeds are no longer required by the orbital elements of family members, however. It has recently been discovered that the Yarkovsky effect can perturb small asteroid orbits significantly over time; see *Bottke et al.* (2002).]

2.2. Regolith All the Way Down

For asteroids larger than ~100 km, another concept was introduced in the 1970s: the existence of gravity-controlled rubble piles that consist of nothing but regolith. In developing an asteroid collisional evolution model, *Davis et al.* (1979) defined a threshold specific energy Q^*_D (impact kinetic energy per target mass) required to both shatter mechanical bonds and accelerate half the mass to escaping trajectories. Shattering requires a lower specific energy $Q^*_S < Q^*_D$ to create fragments none larger than half the target mass. For small rocks $Q^*_D \rightarrow Q^*_S$, whereas for large bodies $Q^*_S/Q^*_D \rightarrow 0$. Whenever $Q^*_S \ll Q^*_D$, the probability of a shattering impact becomes far greater than the probability of a dispersal, in which case an asteroid might be expected to evolve into a pile of rubble, unless other effects (such as melting and compaction) were to dominate.

Davis et al. (1979) expressed impact strength as the sum of the shattering strength plus the gravitational binding energy of the target, for example,

$$Q^*_D = Q^*_S + 4/5\ \pi\ \rho\ GR^2 \qquad (1)$$

where R is the radius of a spherical target and ρ is its density. Equation (1) is called energy scaling; on a graph of Q^*_D vs. R (see Fig. 1) it plots as a horizontal line ($Q^*_D \approx Q^*_S =$ constant) transitioning at some size to a gravity-regime slope of 2 ($Q^*_D \propto R^2$). The size corresponding to this break in slope is known as the strength-gravity transition for catastrophic disruption. [The strength-gravity transition for catastrophic disruption must be distinguished from the strength-gravity transition for planetary cratering. An object in the gravity regime for disruption (Earth is one) can certainly have strength-controlled craters.] Subsequent analysis has

changed the slopes in both regimes (the predicted transition size varies by orders of magnitude from model to model), but the concept was established that beyond some size rubble piles might exist.

Because ρQ_S^* has dimensions of strength and is close to the corresponding static tensile strength of ice and rock in laboratory impact experiments (*Fujiwara et al.,* 1989), tensile strength was used as an easily measured proxy for ρQ_S^* in early disruption theory. Primitive asteroids, comets, and early planetesimals, which are presumably weak, would be easily disrupted. This led to some notable inconsistencies, the most obvious being that primitive bodies smaller than ~100 km would be unlikely to survive over billions of years, in contrast with their abundant population.

The resolution to this dilemma appears to be that impact strength and tensile strength are not simply related, and may even be inversely correlated. Only later did experiments show that loosely bonded aggregates [such as a pile of sintered glass beads (*Love et al.,* 1993)] can survive a projectile that would blast an equal-mass monolithic cylinder to smithereens. It is now believed that some of the most fragile bodies in the solar system — porous aggregates with little or no cohesion — can be highly resistant to catastrophic disruption owing to their ability to dissipate and absorb impact energy. Furthermore, ejection velocities from fragile bodies are correspondingly low, enabling them to hold on to their pieces. Like palm trees that bend in a storm, weak asteroids may survive collisions that would shatter and disperse monolithic solids.

But prior to these and other recent insights to be explored below, a straightforward application of laboratory-derived values for Q_S^* and for the partitioning of impact kinetic energy among fragments (*Fujiwara and Tsukamoto,* 1980) made it fairly obvious that bodies up to ~100 km diameter would be strength-controlled. This fit in well with the idea (*Housen et al.,* 1979; *Veverka et al.,* 1986) that regolith would be thin or absent on such bodies. The ~100-km transition gained further support due to its consistency with two much simpler notions: (1) The transition should occur when central pressure $\sim 2/3\pi G\rho^2 R^2$ equals rock strength; for icy or rocky targets this transition occurs at about 100 km diameter since rock is both stronger and denser. (2) It should occur when gravitational binding energy per volume equals rock strength Y; neglecting constants this yields $R\rho = \sqrt{(Y/G)}$, and R on the order of several hundred kilometers, again whether for ice or rock.

With four distinct ways of viewing asteroid structure converging upon a transition to the gravity regime at ~100-km sizes, the idea seemed safe that all but the largest asteroids were monolithic. Because geochemists predict intense early thermal effects in bodies larger than 100 km (*Scott et al.,* 1989; *McSween et al.,* 2002) the existence of rubble piles remained a conjecture.

2.3. Size-dependent Strength

Impact modelers soon began to appreciate that static strength is sensitive to target size (*Jaeger and Cook,* 1969; *Lawn and Wilshaw,* 1975) because of the greater likelihood of finding large flaws in large volumes. This notion, formalized by engineers who found that it became increasingly difficult to grind coal (for example) down to smaller and smaller sizes, contributes a new power-law size-dependence to asteroid mechanics. Break any brittle solid in two under modest tension, and the number of available flaws decreases by the weakest flaw (plus whatever neighboring flaws are utilized to grow the crack). Continue in this manner to deduce that strength increases monotonically with decreasing size. [The concept was originally demonstrated by measuring the force required to snap smaller and smaller pieces of thread (*Weibull,* 1951)].

If the static failure stress s of a rock decreases with flaw size L as $\sigma \propto 1/\sqrt{L}$ (*Griffith,* 1920), and if the maximum flaw size in a target rock increases in proportion to its radius [as postulated by *Fujiwara* (1980) in his argument for size-dependent strength], then impact strength — if equated with static failure stress — depends on target size R as

$$Q_S^* \propto 1/\sqrt{R} \qquad (2)$$

This same relation was derived by *Farinella et al.* (1982) by relating impact energy to the energy required to form new surface area during fracture. When plotted on a graph of Q_D^* vs. R (Fig. 1) this has a slope of –1/2 in the strength regime: According to this relation (and neglecting strength-selection effects of meteorites, which makes them stronger still), a centimeter-sized meteorite is ~1000× stronger than a 10-km asteroid. This has tremendous implications for the survival of asteroids. If strength diminishes this rapidly, self-gravity becomes the dominant binding force at sizes smaller than previously considered.

A problem crops up at this point: The larger asteroid is only weaker somewhere, otherwise every cubic centimeter of a large asteroid would be weaker than every cubic centimeter of a small asteroid of the same material. To avoid such nonsense, concepts of heterogeneity are required. Instead of considering only the single weakest flaw, consider an asteroid of volume $V \sim R^3$ that samples a theoretical continuum riddled with a power-law distribution of flaws. These can be grain boundaries, pores, inclusions, or cracks opened by previous collisions.

Suppose the number of flaws per unit volume that begin to grow at or below a stress σ is described by a simple power law

$$n(\sigma) = k\sigma^m \qquad (3)$$

The probability (*Weibull,* 1939) of finding a flaw in a random volume V that will begin to grow at or below σ is then $1\text{-}\exp[-(\sigma/\sigma_{min})^m]$, where

$$\sigma_{min} = (kV)^{-(1/m)} \qquad (4)$$

The threshold for failure σ_{min} goes with the –3/m power of radius. For reasons not yet understood, m ~ 6 may be favored by nature (*Housen and Holsapple,* 1999; *Asphaug,*

TABLE 1. Weibull dynamic fracture coefficients for various rocks.

Material	Reference	m	k (cm^{-3})	ln(k)/m
Basalt*	*Melosh et al.* (1992)	9.5	1.0×10^{27}	6.54
Basalt*	*Benz and Asphaug* (1995)	9.0	4.0×10^{29}	7.17
Basalt†	*Lindholm et al.* (1974)	9.5	1.59×10^{30}	7.32
Granite†	*Grady and Lipkin* (1980)	6.2	4.14×10^{17}	6.54
Water Ice*,†,‡	*Benz and Asphaug* (1999)	9.6	1.4×10^{32}	7.71
30% Sand + Water Ice†	*Stewart et al.* (1999)	9.57	1.34×10^{30}	7.25
Concrete†	*Grady and Lipkin* (1980)	5.3	5.27×10^{12}	5.53
Oil Shale†	*Grady and Kipp* (1980)	8.1	1.70×10^{21}	6.04
Limestone†	*Grady and Lipkin* (1980)	57.0	4.26×10^{167}	6.77

* Determined from simulation fits to laboratory data. The two-dimensional axisymmetric simulations of *Melosh et al.* (1992) require stronger fracture parameters than the nonsymmetric three-dimensional simulations of *Benz and Asphaug* (1995) for the same impact experiment.

† Determined experimentally through measurements of tensile strength vs. strain rate.

‡ Earlier published values of m = 8.7, k = 3.2×10^{38} (*Lange and Ahrens,* 1983) were later corrected to similar values [m = 9.57, k = 1.28×10^{32} (*Stewart et al.,* 1999)].

Although k ranges by ~150 orders of magnitude, the situation is not entirely bleak. Homogeneous materials (such as limestone reported below) have large m, and metals are approximated by $m \rightarrow 8$. Because the static failure threshold (σ_{min}) is unchanged so long as ln(k)/m remains constant (see text), homogeneous materials of a given strength have very large k. Equation (4) shows how rocks with large m exhibit little size dependence. While dynamic fracture coefficients have yet to be measured for any meteorite, *Housen and Holsapple* (1999) propose that m ~ 6 might generally describe "well-cracked rocks at large scale," and hence might apply to asteroids.

1993), in which case one recovers equation (2) assuming $Q_S^* \propto \sigma_{min}$. But values of m as high as 57 and as low as 2 have been reported for rocks in the literature (*Grady and Kipp,* 1980) (see Table 1) and no values of m or k have been reported for any meteorite.

In some instances m may be determined by direct measurement of the flaws in a geologic specimen. However, this introduces a bias, as flaw sizes approaching the sample size tend to be excluded, and flaws larger than the sample will not exist. More generally m is determined by fitting laboratory experiments to the strength-strain rate relations described below, although these experiments are limited to small specimens and to the small flaws activated by dynamic fragmentation. In most asteroid impact models, fracture parameters for basalt, granite, or ice are assumed; the sensitivity of these models upon m precludes one from having robust faith in blind forward modeling.

2.4. Rate Dependence

The above analysis of σ_{min} provides a static explanation for why Q_S^* should diminish with size. But Q_S^* is further diminished on account of dynamical fracture mechanics: Rock strength is a function of the loading rate $\dot{\varepsilon} = d\varepsilon/dt$, where ε is the mechanical strain. It has long been established that the dynamic failure strength of rocks scales with the ~1/4 to ~1/3 power of $\dot{\varepsilon}$ (*Rinehart,* 1965). Recognizing that $\dot{\varepsilon}$ decreases with the size of the collisional event, *Holsapple and Housen* (1986) explored the implication of low strain rate collisions in a revised set of scaling models.

If $\dot{\varepsilon}$ is approximated as the impact speed divided by the impactor radius, then a 1-km-diameter impactor striking at 5 km/s couples at a strain rate $\dot{\varepsilon} \sim 10\ s^{-1}$. Though undeniably dynamic, this is a far cry from the $\dot{\varepsilon} \sim 10^6\ s^{-1}$ typical of laboratory experiments. Moreover, stress waves broaden and decay with distance, so $\dot{\varepsilon}$ drops with a steep (~4th) power of distance during hypervelocity collisions (*Melosh et al.,* 1992). Strain rates responsible for shattering of ~10-km asteroids can be as small as 10^{-3} to $10^{-5}\ s^{-1}$ (*Asphaug and Melosh,* 1993).

Grady and Kipp (1980) applied Weibull statistics (equation (3)) to derive a dynamic fragmentation model computing fracture stress and fragment size as a function of $\dot{\varepsilon}$. Except for dynamical loads of such intensity that brittle fragmentation is not the mode of failure, cracks grow at a rate c_g that is about half the sound speed (*Lawn and Wilshaw,* 1975). The crack tip is assumed to accelerate instantaneously to this velocity, when in fact it takes some finite time that depends upon the applied stress and upon crack length. This dependence upon crack length (the integral of crack growth velocity) makes any formal treatment of crack tip acceleration difficult in such models. Because cracks relieve stress over finite time, a dynamic equilibrium is established whereby strong flaws become active as needed, when weaker flaws cannot grow fast enough to accommodate the accumulating stress. Therefore the weakest flaws are sufficient to relieve the stress under low strain rates, resulting in large fragments (due to the low density of weak flaws) and a low measured strength. At high strain rates, on the other hand, stronger and more numerous flaws are

called into play. This leads to the formation of small fragments (because of the high density of strong flaws) and at high measured strength. The resulting relationships (*Grady and Kipp,* 1980) are

$$\sigma \propto \dot{\varepsilon}^{3/(m+3)} \quad (5)$$

where exponents of 1/3 and 1/4 (*Rinehart,* 1965) correspond to m = 6 and m = 9 respectively, and

$$L \propto \dot{\varepsilon}^{-m/(m+3)} \quad (6)$$

so that fragment size L is inversely proportional to strain rate for large m.

These same assumptions are the basis for numerical models of dynamic fracture of brittle solids (*Melosh et al.,* 1992; *Benz and Asphaug,* 1994, 1995), namely that (1) cracks initiate from a Weibull distribution in accordance with the applied tensile stress, (2) the crack tip accelerates instantaneously to half the sound speed, (3) planar cracks of radius a relieve deviatoric and tensile stress in a spherical circumscribed volume; and (4) a volume is damaged (stress-relieved) according to the ratio of cracked volume to total volume. Fully damaged rock, according to these models, is relieved of all stress except compressive pressure, and behaves as a fluid. [A straightforward modification would be to have fully damaged rock behave as a cohesionless Mohr-Coulomb material, where shear stress is still resisted according to the applied normal stress according to the material's angle of internal friction (angle of repose).] Differences in these models depend primarily upon implementation, with *Grady and Kipp* (1980) assuming $\dot{\varepsilon}$ = constant to derive closed integrals, *Melosh et al.* (1992) allowing integration over time-varying strain rate, and *Benz and Asphaug* (1994, 1995) introducing an explicit flaw distribution plus three-dimensional hydrodynamics in addition to time-varying strain rate. [In these numerical models, the total stress tensor is rotated into principal axis coordinates and the maximal value (most tensile) is taken as the stress σ that activates the Weibull flaws.] Without explicit flaws (assigned at random from equation (3) to all discretized volume elements) large rock volumes are modeled as homogeneously weak everywhere, when in fact rock strength is approximately fractal.

Experimental verification of rate dependence in catastrophic collisions was obtained by *Housen and Holsapple* (1999) in a series of experiments involving cylindrical granite targets ranging from 1.9 to 34.4 cm diameter. These targets, identical except for size, were impacted by proportional diameter Al cylinders at uniform speed (~0.6 km/s), with Q^* held constant at ~1.0×10^7 erg/g for each event. The remarkable outcome is shown in Fig. 2. The smallest target is merely chipped by the bullet, while the largest target (everything held constant but size) is catastrophically demolished. *Housen and Holsapple* (1999) found agreement between this granite test data and hydrocode estimates (*Ryan and Melosh,* 1998) for critical specific energy as a function of target size; detailed quantitative comparisons of these specific experiments are in progress.

At low strain rates, not only is strength diminished, but so is ejection velocity. Fragment ejection energy ($1/2 v_{ej}^2$) is proportional to the energy of fragmentation (strength), which varies inversely with target size. Thus, the fragments from a large asteroid travel more slowly, not counting the effects of gravity. This greatly reduced ejection velocity is perhaps the most significant aspect of rate-dependent strength for asteroid collisional evolution, since as $v_{ej} \rightarrow v_{esc}$ self-gravity begins to dominate.

Rate-dependent and size-dependent strength, together with the greatly diminished ejection speeds for large/weak targets, combine to greatly increase gravity's influence over catastrophic disruption for small asteroids. By the early 1990s, rate-dependent scaling theories (notably *Holsapple and Housen,* 1986) had pushed the threshold size for catastrophic disruption down to tens of kilometers diameter. This revised threshold (soon to be pushed to even smaller sizes) began to erode confidence in well-established principles, and placed asteroid science at a crossroads. By 1990 there was no longer any uniformly accepted conclusion regarding asteroid internal structure and the existence of regolith. In only a few years, the first detailed views of asteroids would come along, without science having converged upon even the basics of what they are.

3. CONCEPTS

3.1. Structural Nomenclature

Before proceeding, it is useful to introduce various archetypes for asteroid interiors (see *Richardson et al.,* 2002). Simplest is the monolith, which is any rock of low porosity and significant strength. A monolith is a good transmitter of elastic stress. By definition, monoliths tend to be smaller than the nominal strength-gravity size transition. Since this transition is likely to be dependent upon fracture parameters and ρ (at least), any theoretically abrupt transition would be smoothed out over a population. Monoliths formed by impact ejection from a parent body must be stronger than the acceleration stress; kinetic energy densities and angular momentum densities (speeds and rotation rates) should therefore be high.

Monoliths are fractured by impact bombardment, in which case their tensile strength is compromised and may be reduced to zero (shattered). A fractured or shattered monolith might transmit a compressive stress wave fairly well, provided pore space has not been introduced between the major fragments. (Tensile stress, however, is not supported across a fracture.) A rubble pile includes any shattered body whose pieces are furthermore translated and rotated into loose packing (e.g., *Chapman and Davis,* 1975). Stress waves of any sort are poorly transmitted across a rubble pile, although intense shocks may propagate by crushing and vapor expansion. This category also includes primor-

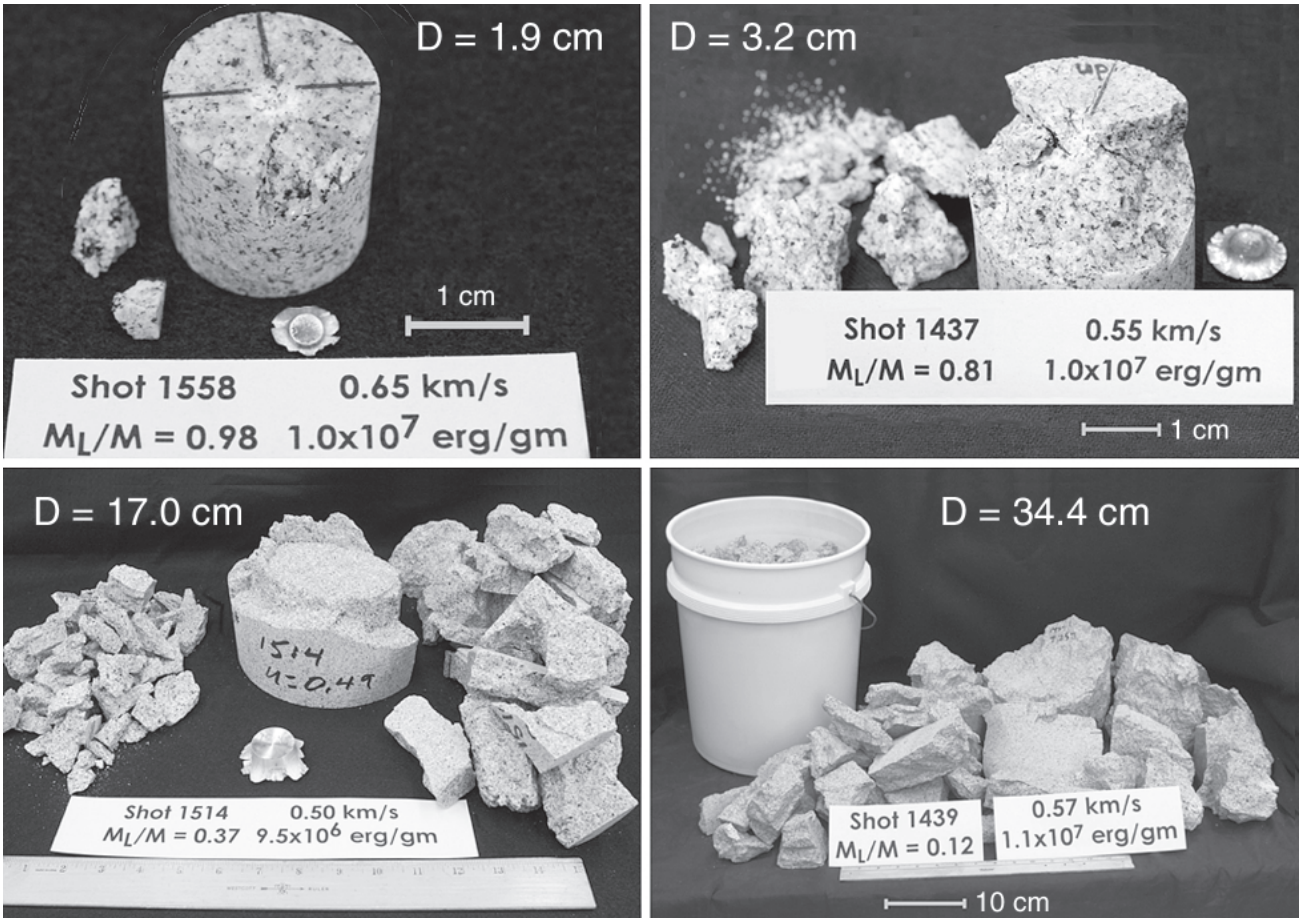

Fig. 2. In a controlled series of impact experiments using a unique ballistics facility at Boeing Aerospace, *Housen and Holsapple* (1999) impacted granite targets ranging from 1.9 cm to 34.4 cm diameter, otherwise identical, with proportional Al bullets fired at ~0.6 km/s, so that $Q^* = 1.0 \times 10^7$ erg/g for each event. The recovered bullet is the "fried egg" next to the first three targets. Because strength is sensitive to both the loading rate and the target size, the mass of the largest remnant drops by a factor >8 between the smallest and largest impacts. Analysis of the fragment size distributions leads to a Weibull exponent m ~ 6 for this material, in agreement with thin-section examinations of the target rock's flaw structure. This change of outcome happens across little more than an order or magnitude in size; imagine the outcome for an ~10-km granite cylinder floating in space. Because rocks get weaker with the ~3/m power of size (see text), asteroids as small as ~1 km are now believed to be gravity-dominated entities.

dial rubble piles, those objects that accreted as uncompacted cumulates. These objects (e.g., *Whipple,* 1949; *Weissman,* 1986) may have formed heterogeneously from grains into clusters, clusters into larger aggregates, and so on hierarchically into comets and asteroids (e.g., *Weidenschilling and Cuzzi,* 1993).

3.2. Onion Shells and Cosmic Sediment

Many asteroids trace their lineage to differentiated protoplanets, and this remains the conceptual model for family-related asteroids (*Hirayama,* 1923; see also *Zappalà et al.,* 2002). Meteoriticists have strong evidence for disrupted parent bodies; the H and L chondrites can be convincingly reassembled (*Keil et al.,* 1994) as "onion shells" of increasing metamorphic grade with depth, and HED achondrites appear to be samples of the crust and upper mantle of asteroid Vesta (*Drake,* 1979; *Binzel and Xu,* 1993; *Asphaug,* 1997; *Keil,* 2002; *Burbine et al.,* 2002). Vesta is the only known survivor of the original "onions" (basalt or related partial melts on the outside, and presumably olivine and then Fe on the inside), so the remainder of the original differentiated asteroids — dozens of parent bodies judging by the number of distinct classes of iron meteorites — have been catastrophically disrupted (see *McSween et al.,* 2002).

In contrast to differentiated asteroids and their monolithic fragments are the rubble piles, which either accreted as cumulates but never metamorphosed, or which reaccreted in the aftermath of a collision when $Q^*_S < Q < Q^*_D$. Indeed, disruption and reaccumulation of planetesimals is likely to have been a common and ongoing process in the early solar system. In a terrestrial context we would call such an

object sedimentary, of local or transported origin — this may be a more appropriate paradigm for asteroids since the igneous "onions" appear to be mostly gone. Indeed, observation and modeling no longer support the idea of simple parentage for most surviving asteroids. For example, M-type spectra are no longer thought to be indicative of metallic composition (see *Rivkin et al.,* 2002). S-type asteroids, apparently primitive in composition (*Trombka et al.,* 2000), appear in some cases (e.g., Gaspra) to derive from much larger parent bodies that one might expect to have undergone extensive metamorphism. Strangest of all is the quandary that olivine-rich materials, representing mantle rocks from the dozens of disrupted original companions to Vesta, is unaccounted for in the meteorite collection (see *Burbine et al.,* 2002), despite the fact that mantle rock should represent at least half of each disrupted parent body's mass.

3.3. Meteorites

Samples of asteroid interiors exist on Earth. However, meteorites remain for the most part "samples without geologic context" (*McSween,* 1999), and any connections between meteorite class and asteroid taxonomy are tentative. To further obscure the asteroid-meteorite relationship, meteorites are small, highly selected specimens whose mechanical (and perhaps compositional) properties are seldom representative of asteroidal parents, as the latter are certainly weaker and more porous (*Flynn et al.,* 1999).

Selection effects prevail when a meteorite is blasted from a parent body. Because strong rock fragments are ejected at the highest speed, strong meteoroids are most likely to leave their parent body at sufficient speed to encounter Earth at 1 AU. Fragments must furthermore survive a long and convoluted journey through space, including the threat of catastrophic disruption by smaller meteoroids (*Greenberg and Nolan,* 1989; *Burbine et al.,* 1996) and must finally survive passage through Earth's atmosphere and then residence upon our planet. They must also wind up in a meteorite collection, although the Antarctic search plus direct followup of fireballs has removed much of the bias against finding extraterrestrial stones that may look like terrestrial rocks.

Only one meteorite parent body to date has been visited with a sample return mission: A comparison of lunar meteorites with Apollo samples (*Warren,* 1994) reveals that lunar meteorites are on the average much stronger than what the astronauts gathered and brought home. Martian meteorites are also highly selected, almost all of them being relatively young basalts, whose high strength and wave speed may have facilitated their acceleration to escape velocity during a cratering event (*Head and Melosh,* 2000).

3.4. Cohesion

A volatile-rich aggregate is more cohesive than a dry aggregate because of the facilitation of mechanical bonding, either directly (e.g., van der Waals forces) or indirectly during episodes of sublimation and frost deposition (*Bridges et al.,* 1996). Some propose the existence of volatile reservoirs in the deep interiors of primitive asteroids, with their mantles depleted through sublimation (*Fanale and Salvail,* 1990) or impact (see *Rivkin et al.,* 2002). For gravity as low as on a typical asteroid, frost or other fragile bonds can be critical to long-term survival during impact or tidal events. Comet Shoemaker-Levy 9, for example, could never have disrupted during its 1992 tidal passage near Jupiter (a nearly parabolic encounter with periapse of 1.3 jovian radii) had the tensile strength across the comet exceeded ~1000 dyn/cm^2 (*Sekanina et al.,* 1994), weaker than snow. *Asphaug and Benz* (1994b, 1996) calculated a maximum tensile strength of only ~30 dyn/cm^2 for Shoemaker-Levy 9 in order for it to fragment from a coherent body into ~20 pieces, and therefore proposed a rubble-pile structure for this comet and gravitational clumping (as opposed to fragmentation) as the cause of its "string of pearls" postperiapse structure. It matters a great deal whether a body is truly strengthless or only extraordinarily weak: Volatile inventory is critical, and poorly known.

3.5. Fast and Slow Rotation

Recent discussion regarding monolithic asteroids has centered around a simple but profound observational result by *Pravec and Harris* (2000; see also *Pravec et al.,* 2002). None of the ~1000 asteroids larger than 150 m with reliably measured spin periods rotates fast enough to require global cohesion. Specifically, for reasonable density estimates none rotates faster than $\omega_o^2 = 4\pi G\rho/3$, where ω_o is the frequency at which material on a sphere's equator becomes orbital. The corresponding minimum rotation period is $P_{crit} = 3.3 \text{ hrs}/\sqrt{\rho}$, with ρ in g/cm^3. The most dense common asteroids (S type) appear to have $\rho \sim 2.7$ g/cm^3 (*Belton et al.,* 1996; *Yeomans et al.,* 2000); thus an S-type gravitational aggregate can spin no faster than $P_{crit} \sim 2.0$ hrs [see *Holsapple* (2002) for a more detailed analysis of rotational breakup]. From the Pravec-Harris asymptote at 2.2 hrs one might infer a common maximum density $\rho \sim 2.3$ g/cm^3, but as few asteroids are spherical the corresponding density is probably greater: Equatorial speeds are faster on an elongated body and the mass distribution is noncentral.

The easiest interpretation is that nearly all asteroids larger than ~150 m lack cohesion. There are other plausible interpretations. Larger asteroids might be internally coherent but possess thick regolith, shedding mass into orbit whenever random spinups [or spinup by the Yarkovsky effect (*Rubincam,* 2000)] cause them to transgress the 2.2-hr rotation period, and then transferring angular momentum to this orbiting material. In this case the ~150-m transition may be the minimum size required for a body to retain regolith, and may have less to do with asteroid internal structure.

Another possibility is angular momentum drain (*Dobrovolskis and Burns,* 1984). Angular momentum is lost whenever prograde ejecta (that launched in the direction of an asteroid's rotation) preferentially escapes while retrograde ejecta remains bound. This is a good explanation for the relatively slow rotations of ~50–100-km-diameter asteroids, but for this process to apply to ~150-m asteroids the ejecta

mass-velocity distribution must have a significant component slower than v_{esc} ~ 5–10 cm/s. Such slow ejection speeds are typical of gravity regime cratering; for craters on ~150-m bodies to be governed by gravity, the target must be strengthless.

A final possibility is that small asteroids are simply collision fragments with more angular momentum per unit mass than the larger remnants. In that case one would anticipate a smooth transition from fast, small rotators to large, slow rotators, whereas the observed transition appears to be abrupt. Furthermore this does not explain the absence of anomalous fast-rotating asteroids larger than 150 m. In summary, the rotation rate data appear to require that asteroids larger than 150 m are either strengthless or else mantled in deep regolith; perhaps future rotation rate surveys around this transition size will constrain our explanations.

An even bigger mystery is that only one asteroid smaller that 150 m diameter (out of ~25 total) with measured rotation rate rotates slower than this limit. [These statistics change on a monthly basis and are by the time of reading out of date; see *Pravec et al.* (2002)]. While no asteroid larger than ~150 m shows evidence for global cohesion, almost all asteroids smaller than this must be cohesive. One might suppose that every larger asteroid is a gravitational aggregate of smaller pieces, whereas every smaller asteroid is a fast-rotating collisional shard. But the term "monolith" for these smallest asteroids is misleading. Consider a spherical object of uniform density ρ rotating with a frequency ω; the mean stress across its equator is ~$R^2\rho\omega^2$. For the well-studied fast rotator 1998 KY26 (*Ostro et al.,* 1999), self-gravity is not capable of holding it together; however, its ~11-min period and ~30-m diameter requires only a tensile strength of ~300 dyn/cm^2 (presuming ρ ~ 1.3 g/cm^3 for this C-type), orders of magnitude weaker than the tensile strength of snow.

3.6. Regolith and Structural Porosity

Besides the rotationally induced regolith loss just considered, a number of fundamental processes can take place in the components and regoliths of shattered and fractured monoliths and rubble piles.

3.6.1. Grain sorting. *Horstman and Melosh* (1989) proposed that regolith might drain into the interior of the martian satellite Phobos in response to block motion during the collision responsible for its large crater Stickney. Over time this process would expose large crustal blocks to the surface as impact-comminuted materials work their way down (*Asphaug and Melosh,* 1993). *Sears and Akridge* (1998) proposed that grains might become compositionally sorted in a regolith rendered dynamic by volatile outflow or meteorite gardening, resulting in iron-silicate fractionation on an unmelted parent body.

Indeed, an asteroid's regolith or a rubble pile's entire mass might be expected to undergo dynamical granular processes (reviewed by *Jaeger et al.,* 1996) on a variety of timescales in response to a variety of perturbations such as impact excavations, vibrations, tides, differential expansion and electrostatic repulsion (*Lee et al.,* 1996). *Asphaug et al.* (2001a) proposed that the extraordinarily high spatial densities of blocks on Eros (*Chapman,* 2001) represent the migration of large blocks through size-sorting dynamics towards the surface. Because size-sorting (e.g. the Brazil-nut effect) may work best in low gravity (*Jiongming et al.,* 1998), it is even possible that the shapes of rubble-piles might be governed by the very largest blocks working their way out towards the lowest gravitational potential.

A different view of particulate dynamics in rubble piles leads to the stacked block model of *Britt and Consolmagno* (2001), whereby regolith drains inwards only until small grains clog the gaps between large blocks. Thereafter a mantle of fine material settles over an interior of large blocks and voids: a body with fairly high bulk density near the surface, and significant interior porosity. These and other ideas regarding size-sorted asteroid structure will remain conjecture until the sciences of granular dynamics and of asteroid geology make significant advances.

3.6.2. Microporosity vs. macroporosity. One must distinguish between macroscopic and microscopic porosity in aggregate materials. An asteroid consisting of quintillions of tiny grains might exhibit considerable cohesion and perhaps support a fractal-like porosity. The total energy of contact bonds divided by the total mass of a granular asteroid (its overall cohesional strength) is inversely proportional to grain diameter, so that a coarse aggregate is weaker than a fine one. On the other hand a highly porous, finely comminuted body can be crushable: cratering on microporous asteroids might be a strange event involving compaction (*Housen et al.,* 1999) rather than ejection.

A coarse rubble pile by contrast would have far fewer contact surfaces distributed over the same total mass, and would therefore behave much differently. *Asphaug et al.,* (1998) used a coarse rubble pile as a starting condition for impact studies, and found that the impact shock wave gets trapped in the impacted components, with few pathways of transmission to neighboring components. Whether an asteroid is macroporous or microporous, stress wave transmission is hindered due to the great attenuation of poorly consolidated rock, making the survival of porous asteroids during impact more likely, as demonstrated by the experiments of *Ryan et al.* (1991) and *Love et al.* (1993) and as illustrated below.

3.7. Overburden Pressures

Small asteroids have correspondingly low internal pressures. Because our geophysical intuition of monoliths and rubble piles is based upon our familiarity with terrestrial landforms, it may be helpful to consider the equivalent depth z_{eq} of a planar stack of the same material, under Earth gravity, for which overburden pressure $\rho g z_{eq}$ is equal to the central pressure in an asteroid of radius R. Solving, this gives

$$z_{eq}(R) = \tfrac{2}{3}\pi G\rho^2 R^2/\rho g = 1.4 \times 10^{-10}\rho R^2 \qquad (7)$$

in cgs units, where g = 980 cm/s^2. For Phobos z_{eq} ~ 3 m with

a central pressure of about 2/3 bar. For Mathilde, z_{eq} ~ 13 m. For Vesta, z_{eq} ~ 3 km. One might anticipate analogous conditions within rock and soil masses at depths on Earth corresponding to equal applied pressure. It is food for thought that the 150-m-diameter transition observed by *Pravec and Harris* (2000) corresponds to a z_{eq} of less than a millimeter, and to a central pressure of less than 100 dyn/cm^2 — one-millionth the tensile strength of rock. It is therefore easy to appreciate the continued resistance to ideas of gravity dominance at such small scales.

The importance for asteroid geology is considerable, as already discussed. For spacecraft exploration these details are also critical: The maximum shear stress supportable by asteroid regolith will be miniscule, in proportion to this vanishingly small normal stress. The behavior of materials at exploration landing sites is likely to be strange compared with the operational test beds here on Earth.

4. COLLISIONAL EVOLUTION

The physical geology of asteroids is largely the aftermath of several global-scale collisions plus a fusillade of smaller impacts; accretion itself is nothing but collisions of a gentler sort. Tides and surface process play a secondary role, at least in the present solar system. As is now believed to be the case for planet formation (*Wetherill,* 1985), accretion and cratering of asteroids may be dominated in terms of energy, mass, and angular momentum contribution by the largest events. For planets, the largest event might trigger core formation (*Tonks and Melosh,* 1992); for asteroids it may determine the interior structure of the body and hence its response to future collisions. If rubble-pile asteroids are resistant to further disruption (*Love et al.,* 1993; *Asphaug,* 1998) then the first noncatastrophic ($Q < Q^*_D$) impact exceeding Q^*_S might therefore determine an asteroid's long-term survival.

As discussed by *Richardson et al*. (2002), the 150-m threshold discovered by *Harris* (1996) and *Pravec and Harris* (2000) had been deduced by hydrocode simulations of asteroid collisions. *Love and Ahrens* (1996), *Melosh and Ryan* (1997), and *Benz and Asphaug* (1999) applied a variety of code and analytical techniques to explicitly derive the values of Q^*_D for asteroids as a function of size. The most detailed of these studies (*Benz and Asphaug,* 1999) applied a laboratory-derived size- and rate-dependent explicit fragmentation model (*Benz and Asphaug,* 1995) together with a postimpact search for the largest surviving clump, whether bound by self-gravity or strength. All these approaches derive a strength-gravity transition, for initially coherent spherical bodies of rock or ice, at a few hundred meters diameter.

Benz and Asphaug (1999) further found an abrupt transition in the structure of the largest remnant after a disruption. For targets smaller than ~1 km (whether rock or ice) suffering catastrophic disruption, the largest surviving remnant consists of a single monolith in their models. For targets larger than ~1 km, on the other hand, the largest surviving remnant is a gravitationally bound aggregate of pieces all much smaller than the target. This is taken as further evidence that the ~150-m Pravec-Harris transition is due to structure, for it appears to hold true for target materials of dissimilar density, thermodynamical behavior, and flaw distribution. Then again, these hydrocode outcomes are for near-threshold disruption of spherical monoliths, whereas actual asteroids have less-pristine original states and more intricate collisional histories. In particular, a detailed analysis of the impact evolution of primordial rubble piles (or a population evolving through myriad hypervelocity collisions) has yet to be conducted. In an initial exploration (see below), *Asphaug et al.* (1998) find that simple variations in target structure (a crack down the middle, for instance) yields dramatically different disruption outcomes. [For low-impact velocities (~10 m/s) typical of planetesimals in the "cold disk" before planet formation, *Benz* (2000) and *Leinhardt et al*. (2000) find that rubble piles are easily dispersed. This suggests a problematic bottleneck at the initial stage of planetary accretion.]

Given that small impacts are more common than large ones, an event of $Q^*_S < Q < Q^*_D$ is expected before catastrophic dispersal ($Q > Q^*_D$). This means that shattering is expected before catastrophic disruption. The end state of collisional evolution of asteroids larger than a few hundred meters is, by this logic, a gravitational aggregate. Those primitive bodies that are rubble piles from the start (e.g., *Weissman,* 1986) probably follow a different disruption scaling than the monolithic rocks simulated by *Ryan and Melosh* (1998) and *Benz and Asphaug* (1999), with shattering energy Q^*_S actually greater for a rubble pile with modest cohesion than for a monolithic rock (*Ryan et al.,* 1991; *Love et al.,* 1993). It remains unclear how the energy for dispersal, Q^*_D, will change for rubble piles, but it appears this, too, will be greater than for monolithic rock. The two current models for impact into porous asteroids differ fundamentally in this regard (*Asphaug and Thomas*, 1999; *Housen et al.,* 1999) (see below), yet both conclude that aggregate bodies resist disruption and dispersal in the hypervelocity regime.

While there is much to be done in understanding the behavior of shattered monoliths and rubble piles, it would appear that such aggregates are the natural end state of asteroids larger than ~1 km.

5. SIMULATING THE GIANT CRATERS

Asteroids suffering catastrophic disruption have lost at least half their volume and bear little sign of their previous incarnation. Those suffering giant craters, by contrast, still exhibit their original shape minus a huge divot or two, and may tell us how their interiors responded. It is hardly a coincidence that most asteroids imaged to date exhibit craters with diameters comparable to their own mean radius; this simply reflects that asteroids are capable of surviving enormous blows with relative impunity, perhaps owing to their unconsolidated interior structure.

Giant craters probe the brink of catastrophic disruption and thereby elucidate impacts at geologic scales — a process masked by gravity on Earth. With three-dimensional

hydrocodes including rate-dependent strength running on powerful computers, one can model the details of their formation. Indeed, because one must resolve both the target and the impactor, large craters are actually easier to model than small ones for a finite target.

Most importantly, impact models can now be tested against targets of asteroidal composition and asteroidal scale. Rather than relying on blind extrapolation from laboratory experiments, we can match the outcomes of detailed impact models against existing giant craters on asteroids. This begins with an asteroid shape model transformed into a simulation grid [for modeling specifics, see *Asphaug et al.* (1996)]. For a giant crater, one must then reconstitute the shape so as to fill in the volume deficit, hopefully leaving a good approximation of the preimpact target. One then makes initial guesses as to interior structure and composition, as these are to be tested. For the impactor, one can assume nominal incidence angle and impact velocity and adopt some value [perhaps that predicted by gravity scaling (*Housen et al.,* 1983)] for the mass. Craters larger than about ~1 km diameter appear to form in the gravity regime for ~10-km monolithic asteroids (*Asphaug et al.,* 1996), so this is frequently a good starting assumption. One can then iterate upon interior geology, and if required, upon the mass and velocity of the impactor, until one arrives at a satisfactory fit to observables: distribution or absence of crater ejecta, global or regional fractures associated with the event, boulder distributions, etc.

Because high-fidelity modeling remains computationally expensive, and data analysis is not yet automated for this kind of inversion, only rough iterations have been performed to date for a handful of asteroids, as presented here.

Fig. 3. A photomosaic of Phobos by the *Viking* Mars orbiter (see *Thomas et al.,* 1979). The large crater Stickney is visible at the upper left, and a number of grooves are prominent. Groove geometry has been shown (*Fujiwara,* 1991) to correlate with impact stress. Phobos is approximately a triaxial ellipsoid with dimensions 19 × 21 × 27 km; Stickney's diameter is ~10 km. Phobos is mysterious for its subsynchronous unstable orbit about Mars, its low density, and the fact that Stickney did not disrupt a satellite inside the Roche limit.

5.1. Phobos

Phobos, the ~22-km-diameter innermost satellite of Mars, was the first small planetary body observed at high resolution (*Veverka and Thomas,* 1979). Its ~10-km crater Stickney was a major curiosity until giant craters were found to be the norm. Indeed, the smaller martian moon Deimos has an even larger crater in proportion to its size (*Thomas,* 1998), although it took decades for this to be acknowledged. Its prevalent fracture grooves (Fig. 3), probably correlated with Stickney (*Thomas et al.,* 1979; *Fujiwara,* 1991), provide an ideal application for strength models.

Using a two-dimensional hydrocode in axisymmetry (*Melosh et al.,* 1992), *Asphaug and Melosh* (1993) attempted to model Stickney as a strength-regime event; i.e., they used *Housen et al.* (1983) to predict the impactor mass required to yield an equal-sized crater in a geologic half-space, and applied this same impactor to Phobos. Not knowing any parameters other than shape and bulk density [~1.95 g/cm^3 was assumed from the recently concluded *Phobos 2* flyby (*Avanesov et al.,* 1989)], they adopted Weibull fracture constants and equations of state for basalt and for water ice, hoping to span the range of possibilities. They first discovered that a strength-scaled impactor (730 m diameter at 6 km/s, for the size-dependent strength of 0.1 kbar) destroyed Phobos (exceeded Q_S^*) and launched most of the impacted hemisphere into orbit, turning Phobos inside-out. This was in stark contrast to the satellite's state of preservation. Using instead a gravity-scaled impactor [230 m diameter at 6 km/s, from *Housen et al.* (1983)], they found that this fragmented more than enough bedrock (whether for icy or rocky targets) to allow an ~10-km crater to evolve into shock-fragmented material. This greatly diminishes the effect of strength control over crater excavation (see *Nolan et al.,* 1996).

Equally significant, the flow field behind the shock in their model had particle velocities consistent with gravity scaling's predictions, with mean flow of a few meters per second throughout the rubble, and an excavation timescale of an hour. *Asphaug and Melosh* (1993) concluded that Stickney was a gravity-regime event, and showed that huge craters on asteroids as small as a few kilometers in diameter should be gravitationally determined. At slow excavation speeds, however, dynamic grain friction begins to play the role envisioned by *Housen et al.* (1983). This is not yet included in any model. Neglecting friction and the influence of Mars, *Asphaug and Melosh* (1993) found that Phobos should be covered by hundreds of meters of Stickney ejecta,

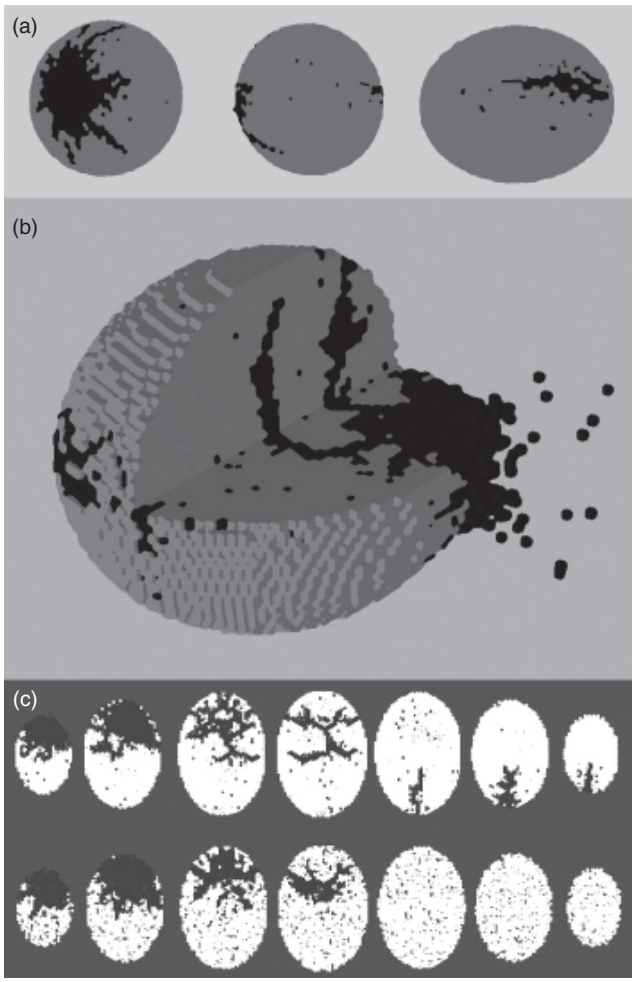

Fig. 4. **(a)** Fracture damage (black) on the surface of an ellipsoidal Phobos viewed during half a rotation, one minute after the Stickney-forming event (*Asphaug and Benz,* 1994a). The initial SPH hydrocode target has a flaw distribution and other material properties (other than density) derived from basalt (used in the absence of better alternatives), substituting a reference density of 1.95 g/cm^3. The impactor is a 230-m-diameter sphere of the same material impacting at 6 km/s. The interior, homogeneous except for the explicit flaw distribution (see text), allows for the transmission of coherent stresses to the backside of the target, leading to focusing and antipodal rupture broadly consistent with observations. **(b)** Cross section through the final Phobos target 12 s after impact. Fast ejecta is escaping, but the crater bowl has only begun to open. An astronaut witnessing the event could read this entire chapter in the meantime. **(c)** Parallel slices 2 km thick through the postimpact targets for two SPH models of Phobos. The top slices show the competent "monolith" with Weibull flaws [**(a)** and **(b)** above], with cracks throughout the cratered hemisphere and at the antipode. The bottom slices show an object of the same bulk density (1.95 g/cm^3) suffering the same impactor, but whose porosity is 30% with material specific density 2.7 g/cm^3. The flecks of black in the bottom slices are interstitial voids (random particles that were removed), not damaged rock. The porous target is a poor transmitter of impact stress; collisional effects are confined to the impacted hemisphere — a crater and little more.

in agreement with observation (*Thomas et al.,* 2000; *Horstman and Melosh,* 1989). Stickney's formation in the gravity regime was dramatically unlike the millisecond-scale laboratory experiments upon which asteroid evolution models had thus far been derived.

Fujiwara (1991) pioneered an important structural geological technique, correlating fracture geometry on small bodies (Phobos) with the responsible impact, thereby constraining elastic mechanical properties of the target rock. More detailed fracture modeling became possible with three-dimensional strength hydrocodes at high resolution, resulting in a kind of asteroid seismology. *Asphaug and Benz* (1994a) performed the same calculations as *Asphaug and Melosh* (1993), but using three-dimensional smooth particle hydrodynamics (SPH), explicit flaws, and an ellipsoidal target (see Fig. 4) so that the actual fracture pattern could be discerned in the model outcome. The modeled Phobos, being a low-density (ρ = 1.95 g/cm^3) elastic solid, transmits stress energy well, and fractures open up radial to the crater and also around the antipode (Fig. 4a). Figure 4b shows ejecta evolution 12 s after impact in this gravity-regime event. One difference between two-dimensional and three-dimensional hydrocode models is that the crater in three dimensions (for the identical gravity-regime projectile) is smaller than in two dimensions. The three-dimensional results show the gravity-regime impactor fragmenting barely enough rock to allow the flow field to open up unencumbered by strength. The discrepancy arises because axisymmetric models cannot relieve stress along radial cracks, resulting in a larger crater bowl. With strength-regime impactors too big and gravity-regime impactors too small, Stickney on Phobos may be intermediate between the classic scaling regimes.

A strongly heterogeneous Phobos was found to be incompatible with groove formation. By removing 30% of the SPH particles at random from a basalt (ρ = 2.7 g/cm^3) target, *Asphaug and Benz* (1994a) constructed a macroscopically porous, highly scattering target of the appropriate bulk density. The top frame of Fig. 4c shows seven "potato chip" slices, 2 km thick, through the final target interior of Fig. 4a. The bottom frame shows the same slices through the 30% porous body (the flecks of black are the interstitial voids). As porous targets are poor transmitters of impact stress, fragmentation is confined to the impacted hemisphere. Phobos cannot have had this kind of highly scattering interior if fracture stresses propagated coherently to the antipode.

With sufficient numerical resolution and time, one might tune the interior model of Phobos to yield the best possible agreement between crack morphologies, crater diameter, ejecta placement, and interior structure. That is the promise of crater profiling of asteroid interiors. At present we arrive at some preliminary conclusions: For either model, the velocities subsequent to impact are too low throughout Phobos to greatly reduce bulk density. If Phobos was not highly porous before Stickney (so that distal cracks could form), and if Stickney did not introduce significant poros-

ity, then the low density of Phobos is compositional or microstructural in nature.

5.2. Ida

By the time *Galileo* encountered asteroid Ida (*Belton et al.,* 1996), model resolution had improved to the point that image-derived shapes could be used in impact simulations. Figure 5 shows an SPH model of Ida based upon the shape derived by *Thomas et al.* (1996): a highly irregular body with mean radius 15.7 km. As with Gaspra (*Carr et al.,* 1994) and Eros (*Prockter et al.,* 2000), this S-type asteroid exhibits expressions of internal shattering in the form of linear furrows almost certainly related to large collisions. Using this Ida model, *Asphaug et al*. (1996) attempted to recreate a few major craters including the ~12-km-diameter Vienna Regio (Fig. 5a). Figure 5b plots particle velocity through a slice of the target 9, 10, and 12 s after a gravity-scaled 330-m-diameter projectile strikes at 3.55 km/s [$\overline{v_{impact}}$ at Ida (*Bottke et al.,* 1994)]. Gravity scaling assumes constant gravity (in this case, the local effective gravity at the impact site) when in fact gravity varies by a factor of ~4 across the asteroid (*Thomas et al.,* 1996), and by a factor of ~2 over the region of this particular collision. Wave interference is complex in this irregular target, and potentially important focusing might occur if the asteroid is a homogeneous transmitter of compressive stress. The simulation (again using fracture and elastic constants for laboratory basalt, pending better alternatives) shows the opening of fractures in the same narrow opposite end of Ida (Pola Regio) where grooves are found. A heterogeneous or porous interior would have dissipated or scattered these stresses (*Asphaug and Benz,* 1994a), so this model outcome lends support to the hypothesis that the deep interior of Ida is competent and homogeneous, in agreement with its presumably low porosity [from its satellite-derived density of 2.6 ± 0.5 g/cm^3 (*Belton et al.,* 1996)]. As with fractured Phobos, mechanical competence is needed only under compression. A well-connected interior is required, but tensile strength is not.

5.3. Eros

The *NEAR Shoemaker* mission to asteroid Eros, completed in 2001, represented a quantum leap for asteroid geology but left deep puzzles about the asteroid's interior. The mission was instrumented to determine asteroid composition, the only interior probe being the radio science experiment, which tracked gravitational influence on orbit

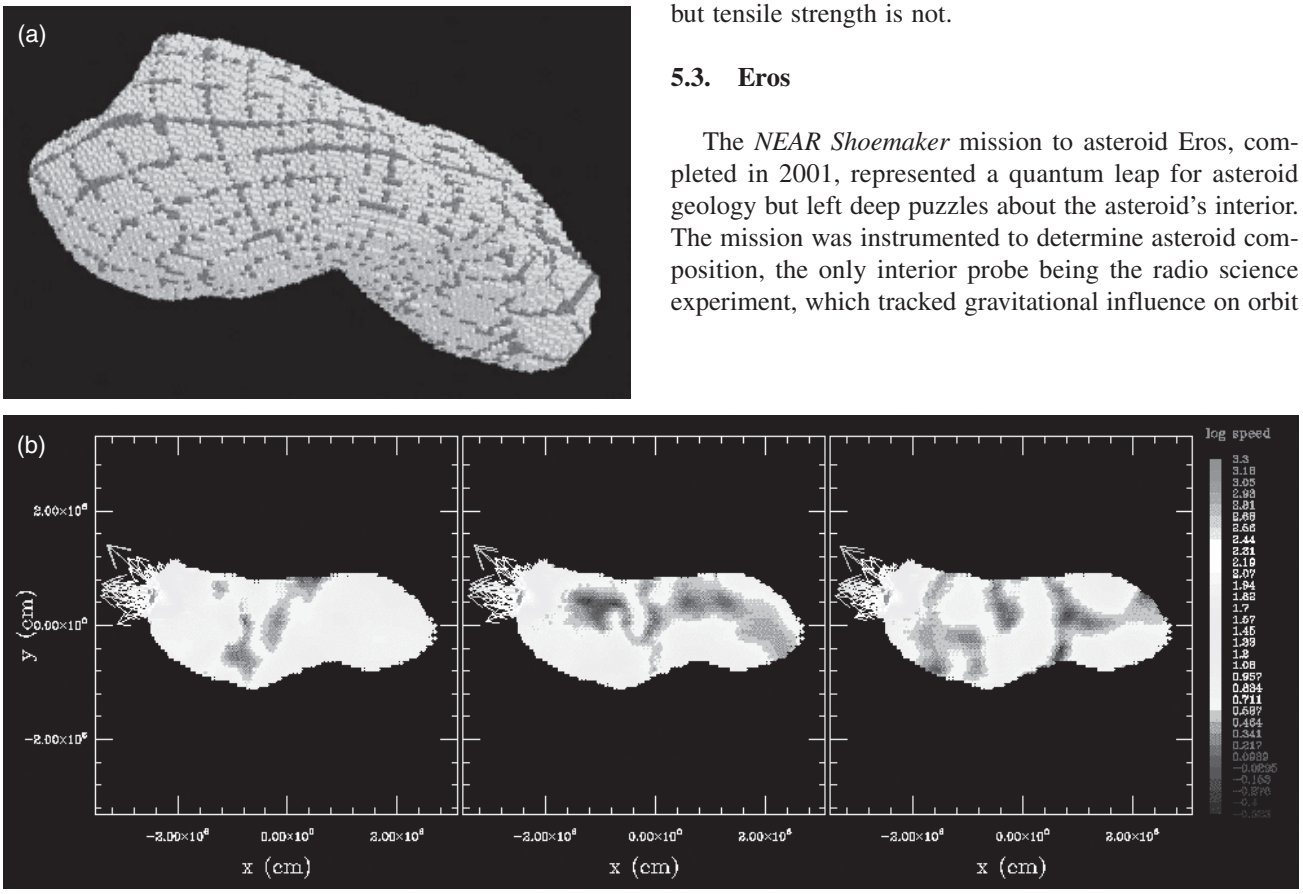

Fig. 5. **(a)** Smooth particle hydrodynamics (SPH) model of asteroid Ida, using the shape derived by *Thomas et al.* (1996) from *Galileo* imaging. This model was used by *Asphaug et al.* (1996) to recreate three major craters on Ida and a suite of smaller craters. Prior to the impact, Vienna Regio (~12-km crater on the upper left) was filled in and then impacted by a gravity-scaled impactor in an attempt to simulate the key aspects of its formation. Particles close to 10° grid lines are color coded in this view. **(b)** Particle velocity is shaded within a slice of the Ida target at t = 8, 9 and 12 s after the 330-m-diameter impactor strikes at 3.55 km/s to create Vienna Regio. Reflections from the complex shape lead to complex waveforms and stress wave interferences as can be seen in the dark zero-velocity nodes. This model resulted in distal, isolated fracture on the far narrow end where grooves are observed, and lent support to the hypothesis that the deep interior of Ida is a good transmitter of compressive stress.

(*Yeomans et al.,* 2000). This enabled determination of density and broad-frequency (approximately kilometer-scale) variations in density; of the latter it found none. Details of this mission are recounted in *Farquhar et al.* (2002); here we consider the implications of these results for asteroid interior structures. In composition and shape, and roughly in size, Eros is akin to Ida, also an S-type with bulk density ~2.7 g/cm^3. This is somewhat lower than the mean density of ordinary chondrites [the closest compositional analog according to *Trombka et al.* (2000)], so Eros is probably as nominally porous as any heavily fractured rock mass. Given its battered appearance (*Prockter et al.,* 2002), Eros' density is not a mystery.

Despite this evidence for disruption, a number of observations exhibit structural competence: the twisted planform of Eros, its clustered regions of high slopes (*Zuber et al.,* 2000), its long, continuous grooves (*Prockter et al.,* 2002), its polygonal craters (indicative of fault structure, just as at Meteor Crater in Arizona), and its subdued or missing crater rims (particularly at the low-gravity ends of the asteroid). The latter suggest crater formation in the strength-regime, where ejecta velocities are higher than v_{esc}. But geological competence is different from dynamical competence, and this has led to a healthy debate about structural nomenclature [perhaps now resolved; see *Richardson et al.* (2002)] and asteroid mechanics.

Nearly all agree the saddle-shaped depression Himeros is an impact crater. Crater fracture models (*Asphaug et al.,* 1996) and seismic profiles at Meteor Crater (*Ackerman et al.,* 1975) show that impact craters have major fractures extending about one crater radius beyond the crater in all directions. For Himeros, fractures would extend through the asteroid's narrow waist. If so, the asteroid is disconnected, possibly evidenced by the complex fault structure Rahe Dorsum, which strikes through Himeros. Dynamicists might then call Eros a "rubble pile" since it comes apart into pieces under modest tension (rotations or tides). To impact modelers, it might fall into that category as well, because a binary object can, like an assemblage of smaller rubble, absorb considerable collisions by trapping impact energy inside the impacted lobe (*Asphaug et al.,* 1998). To reconcile dynamical ideas, that the body might simply float apart if gravity were turned off, with geological ideas, that Eros exhibits considerable strength-controlled structure, we call this S asteroid a shattered monolith, and apply the same term to Ida based upon the modeling just presented.

Despite its irregular shape (see Plate 1) actual slopes on Eros, as on Ida, are moderate. Variations in the gravity vector (including centrifugal force) are extreme, largely canceling extreme variations in topography. One can quantify slopes by plotting a histogram of cumulative area steeper than a given angle (see *Zuber et al.,* 2000), although such histograms depend upon the measurement baseline: Geologic (fractal) surfaces become jagged at small scale. At 100 m baseline, ~2% of Eros is steeper than can be maintained by a pile of talus (see Table 2), and ~3–4% of the slopes are steeper than can be maintained by sand.

TABLE 2. Approximate angles of repose for common materials.

Material	Angle of Repose
Glass beads	~20°
Common unconsolidated materials (e.g., sand)	~33°
Steepest value for highly angular, poorly sorted rocks	~40°–50°
Water-rich soils	up to 90°

Is this evidence for or against structural control? One can argue both ways from the dataset. In order to have some slopes steeper than the presumed angle of repose, Eros must possess some cohesion at ~100-m scales. Conversely, the total area steeper than repose is less than a few percent, and highly localized. Plate 1, derived from the *NEAR Shoemaker* laser rangefinder (NLR) experiment (*Zuber et al.,* 2000), shows these local slopes plotted on a shape model of the asteroid. Almost all slopes exceeding ~30° lie inside the rims of craters, which on Eros (as on the Moon and Earth and other bodies) have slopes consistent with the angle of repose of unconsolidated rock.

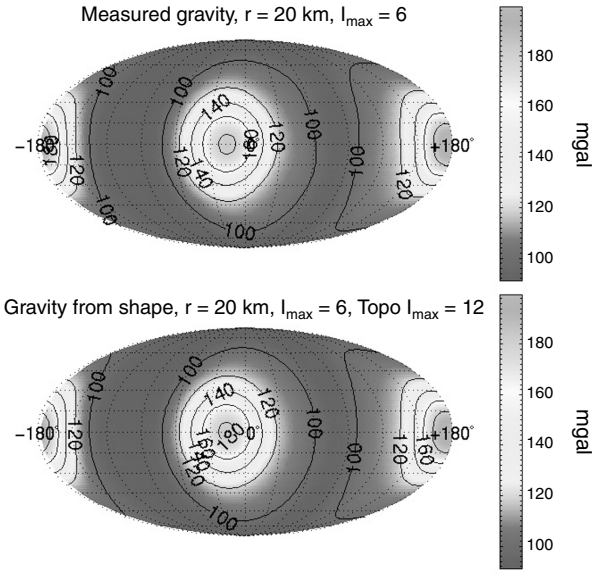

Fig. 6. The *NEAR Shoemaker* gravity experiment (*Yeomans et al.,* 2000) detected no sign of heterogeneity within Eros, as evidenced by these almost indistinguishable gravity maps. The upper figure shows gravity as determined by the radio science experiment, and the lower shows gravity computed from the NLR shape model (*Zuber et al.,* 2000) assuming uniform density. Gravity is only resolved to low degree and order by spacecraft Doppler tracking, corresponding to a resolution at scales of 1 km or larger. Gravity is also more sensitive to exterior than interior components. If Eros is of heterogeneous density, it must be well-mixed at kilometer scales.

The only interior probe of Eros was the radio science experiment that Doppler-tracked the spacecraft position and velocity (*Yeomans et al.,* 2000) and yielded a gravity map of the asteroid's interior. Because orbital speeds were only a few meters per second, intrinsic limits to Doppler accuracy resulted in coarse (approximately kilometer-scale) determination of interior density distribution. Moreover, most of the power in gravity variation is found in the asteroid's exterior, so that interior structure is not well characterized other than bulk density. Figure 6 shows the gravity field of Eros as measured by the spacecraft, plotted at 20 km radius from the center of mass, vs. the gravity field that is deduced from the NLR shape model, assuming a uniform bulk density. The variations are extremely slight, and can be accounted for by tens of meters of regolith thickness variations overlying a uniform substrate, or by a density gradient across the asteroid of 0.006 g cm^{-3} km^{-1}.

Another aspect of Eros is its highly fractured state (*Prockter et al.,* 2002; see also *Sullivan et al.,* 2002), which has been used to support the notion of geologic competence. This dataset also argues both ways. On the one hand it shows that the asteroid can support global fault structures. Conversely, in a dynamical sense, those global fault structures are probably what disconnect the asteroid. The distinction is critical, for as we shall see, an asteroid that is broken behaves very differently during impact than one that is not.

5.4. Mathilde

En route to Eros, *NEAR Shoemaker* encountered the primitive C-type asteroid 253 Mathilde and retrieved high-quality images despite limited solar power and challenging illumination (*Veverka et al.,* 1997) (see Fig. 7a). Mathilde is the first visited of those dark, primitive asteroids that dominate the main belt; it may be typical of unequilibrated or carbonaceous asteroids and perhaps representative of early planetesimals. Orbiting the Sun at a = 2.6 AU, Mathilde measures 66 × 48 × 46 km (best-fit ellipsoid). Its mass, determined by deflection of the spacecraft, is ~1.0×10^{20} g, yielding a bulk density of $\rho \sim 1.3$ g/cm^3, a low density that would be consistent with an icy composition except that groundbased astronomy detects no water on the surface (*Rivkin et al.,* 1997). Mathilde is a typically red C-type asteroid whose spectrum is best matched by primitive carbonaceous meteorites with densities over twice as great, and this has led to the idea of >50% porosity. Mathilde's rotation period is among the longest measured, P = 17.4 d, which is difficult to reconcile with its incredible cratering history: five to seven giant craters, at least four larger in diameter than the asteroid's mean radius, none exhibiting clear signs of structural degradation or overprinting by subsequent collisions, and no evidence for the impact fragmentation that is widespread on Phobos and Eros (*Thomas et al.,* 1999). Regarding the spin period, it is hard to believe (e.g., *Davis,* 1999) that the momentum contribution from all these impacts just happened to cancel out.

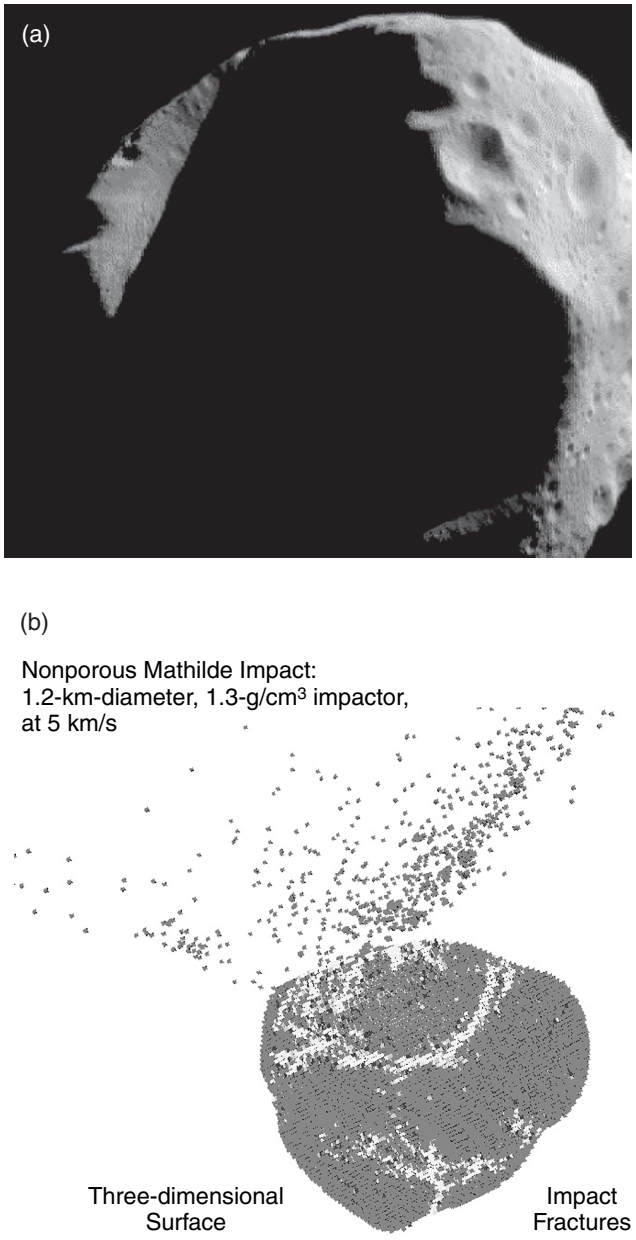

Fig. 7. **(a)** The second image mosaic of asteroid Mathilde (~66 × 48 × 46 km), the only C-type asteroid imaged to date, taken just prior to closest approach (*Veverka et al.,* 1997). Two vast craters span the foreground; there are ~5–7 craters of comparable size (*Thomas et al.,* 1999). Equally baffling are the observations that Mathilde's craters lack raised rims or any other evidence of ejecta deposition, and that Mathilde at ~5 km/pixel shows no sign of fracture grooves, impact disruption, or even rim-disturbance of preexisting craters. Each giant crater left no apparent trace of its formation other than an enormous cavity; we cannot tell which was the last to form. **(b)** A failed attempt using SPH to produce ~33-km-diameter Karoo Crater on Mathilde by introducing a 1.2-km-diameter impactor at 5 km/s (*Asphaug and Thomas,* 1999). The result is a sufficiently large fractured region, but also (as revealed in this side view) widespread impact fragmentation, and bulk ejecta flow velocities slow enough to be gravity-controlled. The result is a seriously fragmented asteroid covered in gravity-regime ejecta deposits — the opposite of what is observed.

Following *NEAR Shoemaker*'s determination of Mathilde's low density, a half dozen primitive asteroids have been found to have similar densities, computed from orbital periods of their newly discovered companion satellites (see *Merline et al.,* 2002). Once density is known, structure and composition are inseparable, since molecular weight then depends on the distribution of voids. Along with previous determinations of low density for the martian moons and Comets Halley and Shoemaker-Levy 9 (*Sagdeev et al.,* 1987; *Asphaug and Benz,* 1994b), these low C-type asteroid densities support a consensus that primitive small bodies are highly porous — rubble piles, primordial aggregates, or volatile-depleted residues. Whatever the origin of a body's porosity, it is significant to impact mechanics (*Trucano and Grady,* 1995) and the topic must be revisited.

The absence of ejecta deposits around a crater can signify formation in the strength regime. Despite earlier modeling to the contrary for a much smaller low-density body, Phobos (*Asphaug and Melosh,* 1993), a strength-regime crater model was attempted for Mathilde by *Asphaug and Thomas* (1998) and the result is shown in Fig. 7b. As in Fig. 4c for Phobos, a size-dependent strength was computed for Mathilde's volume, the largest crater Karoo was filled in, and a strength-scaled impactor (1.2 km diameter) was introduced at 5 km/s into the 1.3-g/cm^3 continuum. The result can be seen as a fractured region larger than Karoo, and also as widespread impact fragmentation all around the asteroid. Nevertheless, flow velocities within the resultant crater are slow enough to be gravity controlled, as they were for Stickney. The result is a globally fragmented asteroid covered in gravity-regime ejecta deposits — entirely the opposite of observation. A bold modeler might remedy this by making Mathilde stronger than basalt, but primitive meteorites are weak, often falling apart in one's hands.

5.4.1. Survival of the weakest. An alternative has emerged from these failed attempts: Perhaps Mathilde is too weak to be disrupted by collisions. This scenario (*Asphaug,* 1999) is borrowed from armament lore, and has roots in the experimental literature (*Love et al.,* 1993). *Davis* (1999), commenting upon Mathilde, recounts the use of porous cactus ribs to dissipate the energy of cannon balls colliding into the walls of Sonoran forts. Perhaps a similar heterogeneity or porosity has enabled Mathilde to survive each giant cratering event without any noticeable disturbance to its preexisting morphology.

The effects of structure and prefragmentation on collisional evolution was examined by *Asphaug et al.* (1998), following the work on asteroid porosity by *Asphaug and Benz* (1994a) and motivated by the experimental work of *Ryan et al.* (1991) and *Love et al*. (1993). For these simulations, shown in Plate 2a, the approximately kilometer-sized near-Earth asteroid Castalia (*Ostro et al.,* 1990) was rendered in a variety of ways: a monolith, a contact binary, and a rubble-pile. Each target was impacted by the same projectile (16 m diameter, 2.7 g/cm^3, 5 km/s) whose kinetic energy happened to equal the yield of one Hiroshima bomb. (This work was published the same week as the release of the Hollywood blockbuster *Deep Impact,* in which brave astronauts use nuclear devices to blow up a rogue comet, so the comparison was unfortunate.) This modeling showed what laboratory studies had hinted at: that monolithic asteroids are actually easier to disperse than rubble piles or gravitational aggregates. The contact binary (not shown) trapped impact energy in the impacted lobe, reflecting it at the discontinuity and preventing any severe perturbation of the distal lobe.

The same modeling technique was used to assemble Mathilde out of basalt spheres (Plate 2b) ranging in diameter from 0.5 to 3 km, just touching, with bulk porosity ~0.5 and bulk density ~1.3 g/cm^3, this time using the material density of basalt (2.7 g/cm^3). Resolving shock waves in each sphere requires a resolution of ~1000 particles per component, requiring supercomputer modification of the code. This places approximately six particles across each component's radius. Because numerical shock waves cannot be treated with fewer than three zones (*von Neumann and Richtmyer,* 1950), that is probably a safe minimum for such simulations. The contact portion of touching spheres is replaced with damaged rock of slightly lower material density (1.7 g/cm^3) and can be seen as red flecks in the bottom of the center figure. Damaged rock cannot support tensile or shear stress, so the modeled Mathilde is just like a contact binary, only with thousands of components. The size of the component spheres is established by the resolution requirement of modeling each individual sphere by ~1000 particles, not by any guiding philosophy of rubble pile structure.

A shock wave can propagate freely through a rubble pile so long as it melts, vaporizes, or collapses pores in the rock it encounters. But shocks attenuate rapidly even in competent rock (*Rodionov et al.,* 1972), and even the most powerful elastic wave has difficulty propagating in an aggregate. Stress energy is trapped, and as a result the impact energy is confined to a local region (the shattered region colored red in the central figure of Plate 2b), so this receives all the energy that would have otherwise been transmitted to distant regions.

Ejection velocities (left) in the damaged region (middle) are therefore greater due to this energy confinement. Indeed, the nonescaping fraction (right) equals all the damaged rock. The conclusion is that structural porosity can lead to stalled shocks, and hence crater ejecta in a weak asteroid, just as in a strength-controlled asteroid, might never return to the asteroid. Furthermore, because almost no stress energy propagates beyond the crater bowl, preexisting craters on Mathilde would not feel the occurrence of subsequent large impacts, and would preserve their original forms, as observed in the *NEAR Shoemaker* images.

5.4.2. Compaction cratering. An alternative model for cratering on Mathilde has very different implications for asteroid structure and evolution. *Housen et al.* (1999) propose that Mathilde is so underdense that craters form by crushing rather than ejection. In their model no ejecta leaves the crater — just opposite the previous scenario in which

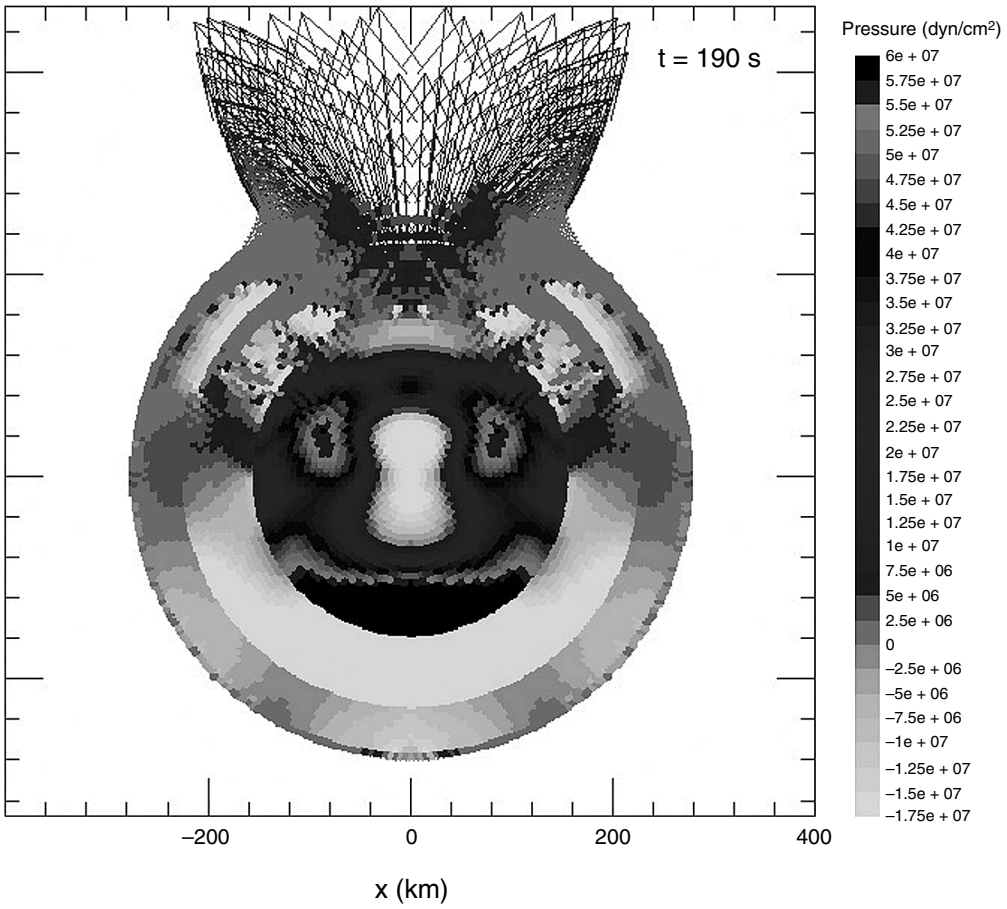

Fig. 8. An impact into the differentiated ~530-km-diameter asteroid Vesta using the two-dimensional hydrocode of *Melosh et al.* (1992). In this calculation a 34-km-diameter impactor strikes at 8 km/s in an attempt to reproduce the hemispheric crater on Vesta and the V-type asteroids (*Asphaug,* 1997; *Keil,* 2002). It turns out to be relatively easy to launch crustal meteorites from parent bodies at high speed, whereas excavation of interior Fe requires truly gargantuan events. Interestingly, much of the stress energy (shown here three minutes after impact as the primary wave reflects from the core/mantle boundary) is trapped in the asteroid's core, reverberating for the remainder of the calculation.

all ejecta leaves the crater. Under compaction cratering, an asteroid crushes up to higher density over time, leaving mass concentrations at each crater floor. Compaction cratering, if it occurs, would have facilitated planetary growth, as it allows primitive asteroids to accrete material with ease. That is also its problem, however, given Mathilde's near-absence of spin. In a regime of perfectly inelastic collisions (see *Agnor et al.,* 1999) accreting bodies almost always begin to spin with periods of hours, not tens of days.

6. LARGER ASTEROIDS

Little has been said in this chapter about larger asteroids, those that have differentiated into cores, mantles, and crusts. For these, meteoriticists would like impact modelers to help them remove their mantles so as to expose their iron cores and deliver iron meteorites to Earth, while at the same time getting rid of mantle material not evident in the meteorite collection (see *Burbine et al.,* 2002). This has proven to be a difficult prospect.

While large asteroid interiors are treated in other chapters in this book (*McSween et al.,* 2002; *Keil,* 2002), one aspect is worth mentioning in passing — that cores can trap impact stress energy in a manner reminiscent of how contact binaries trap energy in their impacted lobe. Figure 8 shows an impact simulation where asteroid Vesta (*Asphaug,* 1997) is modeled using the two-dimensional hydrocode of *Melosh et al.* (1992) to resolve a basaltic crust, a denser mantle, and an iron core. The impact (an attempt to recreate the hemispheric crater on Vesta and the V-type asteroids) transmits a shock deep into the asteroid, where it reverberates throughout the course of the calculation.

7. SEISMIC AND RADAR IMAGING OF ASTEROID INTERIORS

Geophysical exploration tools that are commonly deployed on Earth can be flown on spacecraft to image asteroid interiors directly. Many are designed for field deployment in remote areas and are compact and lightweight.

Radio reflection tomography (ground-penetrating radar or GPR) is commonly used to image sinkholes, pipes, burial grounds, etc.; similar imaging is in principle obtainable on asteroids, although the instruments would probably have to be deployed from orbit, reducing resolution and posing challenges with regard to data inversion and echo noise. The European Space Agency's *Rosetta* spacecraft will use transmission radio tomography (*Kofman et al.,* 1998) to investigate the interior of Comet Wirtanen during its 2011–2016 rendezvous as the comet approaches perihelion; in this mode of exploration radio energy is transmitted from a lander and received by the orbiter. Another popular field-deployable tool, magnetotelluric imaging, probes subsurface geology using the fact that the magnetic to electric-field ratio (impedance) is constant at given frequency for constant resistivity. On Earth this technique takes advantage of natural fluctuations in the background magnetic field, whereas on an asteroid field generation would require the deployment of antennae across the surface.

Certain asteroid materials (clays, rocks flecked with metal) may be opaque to electromagnetic energy and might be better explored by other means. *Deep Impact,* a NASA Discovery mission, will pioneer the technique of kinetically blasting holes in small bodies [*Belton and A'Hearn* (1999); see *Farquhar et al.* (2002) for an overview of recent and planned small-body missions]. In July 2005, *Deep Impact* will slam ~350 kg of copper into Comet Tempel 1 at ~10 km/s for the purpose of investigating outer crust and mantle physical and compositional properties.

A more refined technique, more complex to deploy, is seismic imaging. This has taught us the detailed structure of Earth, and more recently has been refined for small-scale imaging (e.g., *Wu and Yang,* 1997). Seismic imaging may prove to be an ideal complement to electromagnetic imaging of asteroid interiors, since its spatial resolution can be comparable but its means of data acquisition and inversion are entirely distinct. In some cases where seismic imaging is challenging (highly attenuative porous bodies such as comets) radio imaging may be optimal, and perhaps vice versa.

Seismic imaging requires surface probes. In one scenario instrumented penetrators detect signals broadcast from cratering grenades. Blasts produce white noise and are not optimal for tomographic data inversion (compared with drills or thumpers), but they are convenient, reliable, and cheap. They also produce small-scale cratering experiments as a bonus, enabling the imaging and spectroscopy of shallow layers. Alternatively, and at much lower cost, an armada of ballistic penetrators could be deployed to strike an asteroid in the manner that the pieces of Comet Shoemaker-Levy 9 struck Jupiter, hitting it one after another, with each embedded penetrator acquiring seismic reverberations from successive impacts at diverse locations.

One can deploy, at the NASA Discovery level, a dual-wavelength radar tomography mission pursuing multiple rendezvous with a variety of near-Earth objects (*Asphaug et al.,* 2001b). This population is fairly representative of the asteroid population at large, and may include dormant comet nuclei (see *Morbidelli et al.,* 2002; *Weissman et al.,* 2002). Anchored seismology landers would be too costly, given the surface material uncertainties. Spring-fired grenades (a precursor to seismic studies) would blast several small (~5-m) craters at selected sites on each asteroid or comet nucleus. Ejecta ballistics and crater formation filmed from orbit at high time and spatial resolution would facilitate the development of comet- and asteroid-analog simulation chambers at impact research laboratories. Together with long-term imaging of ejecta orbital evolution, this would greatly reduce uncertainties and design parameters for future landed spacecraft.

Until we proceed with direct geophysical exploration of asteroids and comets, our understanding of their interiors shall remain a matter of educated speculation. Science aside, there are practical reasons to learn more in the short term. To divert or disrupt a potentially hazardous near-Earth asteroid, one must understand its internal structure, as porous or discontinuous asteroids can absorb or divert disruptive energy. Composite targets appear to be able to sacrifice small regions near an impact or explosion without perturbing disconnected regions. Monoliths, rubble piles, and porous ice-dust mixtures might each require a different mode of diversion, disruption, or resource exploitation (*Huebner and Greenberg,* 2000). Except for the mean densities of a dozen asteroids and the broadly resolved homogeneous mass distribution of Eros, we know none of the basic bulk constitutive properties of any asteroid. Obviously the modeling presented here is fraught with guesswork. Lacking such knowledge, a standoff blast (*Ahrens and Harris,* 1992) might fail to impart the expected momentum or might disrupt a body without diverting it, sending a cluster of fragments toward Earth. Nonnuclear scenarios (*Melosh et al.,* 1994) are greatly preferred, but these also require detailed awareness of asteroid geology and composition for the purposes of anchoring, momentum loading, and resource extraction.

8. CONCLUSIONS

Asteroids include about a million objects between ~100 m and ~100 km across. Many have satellites (see *Merline et al.,* 2002), and they have long served as test particles for understanding the detailed evolution of planetary dynamics (see *Gladman et al.,* 1997). Their geophysics is a complex interplay between long- and short-range forces (self-gravity and mechanical cohesion), making Earth-based intuition a fickle guide, yet until we peer inside an asteroid directly we can only strive to interpret their exterior geology.

We presently believe that most asteroids larger than ~1 km are gravitational aggregates. Highly tentative is our conclusion that Gaspra, Ida, Eros (all S-types), and perhaps Phobos are shattered monoliths sufficiently competent to transmit compressive stress. As for Mathilde and other low-density primitive bodies, detailed explanations diverge, but

they appear to require a mechanically uncoupled interior, either structural or microstructural. Their porosity may be primordial or the aftermath of collisional evolution; it helps them withstand the gargantuan collisions that have been the norm in the evolving solar system.

There is much to learn. Our present state of knowledge comes as no surprise, for complex characteristics are expected of objects at the boundary between primary forces of nature.

REFERENCES

Agnor C. B., Canup R. M., and Levison H. F. (1999) On the character and consequences of large impacts in the late stage of terrestrial planet formation. *Icarus, 142,* 219–237.

Ahrens T. J. and Harris A. W. (1992) Deflection and fragmentation of near-earth asteroids. *Nature, 360,* 429–433.

Asphaug E. (1993) Dynamic fragmentation in the solar system. Ph.D. thesis, Univ. of Arizona, Tucson.

Asphaug E. (1997) Impact origin of the Vesta family. *Meteoritics & Planet. Sci., 32,* 965–980.

Asphaug E. (1999) Survival of the weakest. *Nature, 402,* 127–128.

Asphaug E. and Benz W. (1994a) The surface and interior of Phobos (abstract). In *Lunar and Planetary Science XXV,* pp. 43–44. Lunar and Planetary Institute, Houston.

Asphaug E. and Benz W. (1994b) Density of Comet Shoemaker-Levy-9 deduced by modelling breakup of the parent rubble pile. *Nature, 370,* 120–124.

Asphaug E. and Benz W. (1996) Size, density, and structure of Comet Shoemaker-Levy 9 inferred from the physics of tidal breakup. *Icarus, 121,* 225–248.

Asphaug E. and Melosh H. J. (1993) The Stickney impact of Phobos: A dynamical model. *Icarus, 101,* 144–164.

Asphaug E. and Thomas P. C. (1999) Modeling mysterious Mathilde (abstract). In *Lunar and Planetary Science XXX,* Abstract #2028. Lunar and Planetary Institute, Houston (CD-ROM).

Asphaug E., Moore J. M., Morrison D., Benz W., Nolan M. C., and Sullivan R. J. (1996) Mechanical and geological effects of impact cratering on Ida. *Icarus, 120,* 158–184.

Asphaug E., Ostro S. J., Hudson R. S., Scheeres D. J., and Benz W. (1998) Disruption of kilometre-sized asteroids by energetic collisions. *Nature, 393,* 437–440.

Asphaug E., King P. J., Swift M. R., and Merrifield M. R. (2001a) Brazil nuts on Eros: Size-sorting of asteroid regolith (abstract). In *Lunar and Planetary Science XXXII,* Abstract #1708. Lunar and Planetary Institute, Houston (CD-ROM).

Asphaug E., Belton M. J. S., and Kakuda R. Y. (2001b) Geophysical exploration of asteroids: The Deep Interior Mission concept (abstract). In *Lunar and Planetary Science XXXII,* Abstract #1867. Lunar and Planetary Institute, Houston (CD-ROM).

Avanesov G.A. and 39 colleagues (1989) Television observations of Phobos. *Nature, 341,* 585–587.

Belton M. J. S. and A'Hearn M. F. (1999) Deep sub-surface exploration of cometary nuclei. *Adv. Space Res., 24,* 1175–1183.

Belton M. J. S. and 20 colleagues (1996) The discovery and orbit of 1993 (243)1 Dactyl. *Icarus, 120,* 185–199.

Benz W. (2000) Low velocity collisions and the growth of planetesimals. *Space Sci. Rev., 92,* 279–294.

Benz W. and Asphaug E. (1994) Impact simulations with fracture: I. Method and tests. *Icarus, 107,* 98–116.

Benz W. and Asphaug E. (1995) Simulations of brittle solids using smooth particle hydrodynamics. *Comput. Phys. Commun., 87,* 253–265.

Benz W. and Asphaug E. (1999) Catastrophic disruptions revisited. *Icarus, 142,* 5–20.

Binzel R. P. and Xu S. (1993) Chips off of asteroid 4 Vesta — Evidence for the parent body of basaltic achondrite meteorites. *Science, 260,* 186–191.

Bottke W. F., Nolan M. C., Greenberg R., and Kolvoord R. A. (1994) Collisional lifetimes and impact statistics of near-Earth asteroids. In *Hazards Due to Comets and Asteroids* (T. Gehrels et al., eds.), pp. 337–357. Univ. of Arizona, Tucson.

Bottke W. F. Jr., Vokrouhlický D., Rubincam D. P., and Brož M. (2002) The effect of Yarkovsky thermal forces on the dynamical evolution of asteroids and meteoroids. In *Asteroids III* (W. F. Bottke Jr. et al., eds.), this volume. Univ. of Arizona, Tucson.

Bridges F. G., Supulver K. D., Lin D. N. C., Knight R., and Zafra M. (1996) Energy loss and sticking mechanisms in particle aggregation in planetesimal formation. *Icarus, 123,* 422–435.

Britt D. T. and Consolmagno G. J. (2001) Modeling the structure of high porosity asteroids. *Icarus, 152,* 134–139.

Bunch T. E. and Rajan R. S. (1988) Meteorite regolith breccias. In *Meteorites and the Early Solar System* (J. F. Kerridge and M. S. Matthews, eds.), pp. 144–164. Univ. of Arizona, Tucson.

Burbine T. H., Meibom A., and Binzel R. P. (1996) Mantle material in the main belt: Battered to bits? *Meteoritics & Planet. Sci., 31,* 607–620.

Burbine T. H., McCoy T. J., Meibom A., Gladman B., and Keil K. (2002) Meteoritic parent bodies: Their number and identification. In *Asteroids III* (W. F. Bottke Jr. et al., eds.), this volume. Univ. of Arizona, Tucson.

Carr M. H., Kirk R. L., McEwen A., Veverka J., Thomas P., Head J. W., and Murchie S. (1994) The geology of Gaspra. *Icarus, 107,* 61.

Cellino A., Michel P., Tanga P., Zappalà V., Paolicchi P., and Dell'Oro A. (1999) The velocity-size relationship for members of asteroid families and implications for the physics of catastrophic collisions. *Icarus, 141,* 79–95.

Chapman C. R. (1976) Asteroids as meteorite parent bodies: The astronomical perspective. *Geochim. Cosmochim. Acta, 40,* 701–719.

Chapman C. R. (2001) Eros at very high resolution: Meteoritical implications (abstract). *Meteoritics & Planet. Sci., 36,* A39.

Chapman C. R. and Davis D. R. (1975) Asteroid collisional evolution — Evidence for a much larger early population. *Science, 190,* 553.

Chapman C. R., Paolicchi P., Zappala V., Binzel R. P., and Bell J. F. (1989) Asteroid families: physical properties and evolution. In *Asteroids II* (R. P. Binzel et al., eds.), pp. 386–415. Univ. of Arizona, Tucson.

Davis D. R. (1999) The collisional history of asteroid 253 Mathilde. *Icarus, 140,* 49–52.

Davis D. R., Chapman C. R., Greenberg R., Weidenschilling S. J., and Harris A. W. (1979) Collisional Evolution of asteroids: Populations, rotations and velocities. In *Asteroids* (T. Gehrels, ed.), pp. 528–557. Univ. of Arizona, Tucson.

Davis D. R., Chapman C. R., Weidenschilling S. J., and Greenberg R. (1985) Collisional history of asteroids: Evidence from Vesta and Hirayama families. *Icarus, 62,* 30–53.

Dobrovolskis A. R. and Burns J. A. (1984) Angular momentum drain — A mechanism for despinning asteroids. *Icarus, 57,* 464–476.

Drake M. J. (1979) Geochemical evolution of the eucrite parent body: Possible nature and evolution of asteroid 4 Vesta? In *Asteroids* (T. Gehrels, ed.), pp. 765–782. Univ. of Arizona, Tucson.

Durda D. D., Greenberg R., and Jedicke R. (1998) Collisional models and scaling laws: A New interpretation of the shape of the main-belt asteroid size distribution. *Icarus, 135,* 431–440.

Fanale F. P. and Salvail J. R. (1990) Evolution of the water regime of Phobos. *Icarus, 88,* 380–395.

Farinella P., Paolicchi P, and Zappalà V. (1982) The asteroids as outcomes of catastrophic collisions. *Icarus, 52,* 409–433.

Farquhar R., Kawaguchi J., Russell C., Schwehm G., Veverka J., and Yeomans D. (2002) Spacecraft exploration of asteroids: The 2001 perspective. In *Asteroids III* (W. F. Bottke Jr. et al., eds.), this volume. Univ. of Arizona, Tucson.

Flynn G. J., Moore L. B., and Klöck W. (1999) Density and porosity of stone meteorites: Implications for the density, porosity, cratering, and collisional disruption of asteroids. *Icarus, 142,* 97–105.

Fujiwara A. (1980) On the mechanism of catastrophic destruction of minor planets by high-velocity impact. *Icarus, 41,* 356–364.

Fujiwara A. (1991) Stickney-forming impact on Phobos: Crater shape and induced stress distribution. *Icarus, 89,* 384–391.

Fujiwara A. and Tsukamoto A. (1980) Experimental study on the velocity of fragments in collisional breakup. *Icarus, 44,* 142–153.

Fujiwara A., Cerroni P., Davis D. R., Ryan E. V., Di Martino M., Holsapple K., and Housen K. (1989) Experiments and scaling laws for catastrophic collisions. In *Asteroids II* (R. P. Binzel et al., eds.), pp. 240–265. Univ. of Arizona, Tucson.

Gault D. E. and Heitowit E. D. (1963) The partition of energy for hypervelocity impact craters formed in rock. *Proc. 6th Hypervelocity Impact Symposium, Vol. 2,* pp. 419–456.

Gault D. E., Horz F., and Hartung J. B. (1972) Effects of microcratering on the lunar surface. *Proc. Lunar Sci. Conf. 3rd,* pp. 2713–2734.

Gladman B. J., Migliorini F., Morbidelli A., Zappalà V., Michel P., Cellino A., Froeschlé C., Levison H. F., Bailey M., and Duncan M. (1997) Dynamical lifetimes of objects injected into asteroid belt resonances. *Science, 277,* 197–201.

Grady D. E. and Kipp M. E. (1980) Continuum modeling of explosive fracture in oil shale. *Intl. J. Rock Mech. Min. Sci. Geomech. Abstr., 17,* 147–157.

Grady D. E. and Lipkin J. (1980) Criteria for impulsive rock fracture. *Geophys. Res. Lett., 7,* 255–258.

Greenberg R. and Nolan M. C. (1989) Delivery of asteroids and meteorites to the inner solar system. In *Asteroids II* (R. P. Binzel et al., eds.), pp. 778–804. Univ. of Arizona, Tucson.

Griffith A. A. (1920) The phenomena of rupture and flow in solids. *Philos. Trans. R. Soc. London, A221,* 163–198.

Harris A. W. (1996) The rotation rates of very small asteroids: Evidence for "rubble pile" structure (abstract). In *Lunar and Planetary Science XXVII,* p. 493. Lunar and Planetary Institute, Houston.

Head J. N. and Melosh H. J. (2000) Launch velocity distribution of the martian clan meteorites (abstract). In *Lunar and Planetary Science XXXI,* Abstract #1937. Lunar and Planetary Institute, Houston (CD-ROM).

Hirayama K. (1923) Families of asteroids. *Ann. Tokyo Astron. Obs., 11,* 55.

Holsapple K. A. (1994) Catastrophic disruptions and cratering of solar system bodies: A review and new results. *Planet. Space Sci., 42,* 1067–1078.

Holsapple K. A. (2002) Equilibrium configurations of solid cohesionless bodies. *Icarus,* in press.

Holsapple K. A. and Housen K. R. (1986) Scaling laws for the catastrophic collisions of asteroids. *Mem. Soc. Astron. Ital., 57,* 65–85.

Holsapple K., Giblin I., Housen K., Nakamura A., and Ryan E. (2002) Asteroid impacts: Laboratory experiments and scaling laws. In *Asteroids III* (W. F. Bottke Jr. et al., eds.), this volume. Univ. of Arizona, Tucson.

Housen K. R. and Holsapple K. A. (1990) On the fragmentation of asteroids and planetary satellites. *Icarus, 84,* 226–253.

Housen K. R. and Holsapple K. A. (1999) Scale effects in stength-dominated collisions of rocky asteroids. *Icarus*, in press.

Housen K. R., Wilkening L. L., Chapman C. R., and Greenberg R. (1979) Asteroidal regoliths. *Icarus, 39,* 317–351.

Housen K. R., Schmidt R. M., and Holsapple K. A. (1983) Crater ejecta scaling laws: Fundamental forms based on dimensional analysis. *J. Geophys. Res., 88,* 2485–2499.

Housen K. R., Holsapple K. A., and Voss M. E. (1999) Compaction as the origin of the unusual craters on the asteroid Mathilde. *Nature, 402,* 155–157.

Horstman K. C. and Melosh H. J. (1989) Drainage pits in cohesionless materials: Implications for the surface of Phobos. *J. Geophys. Res., 94,* 12433–12441.

Huebner W. F. and Greenberg J. M. (2000) Needs for determining material strengths and bulk properties of NEOs. *Planet. Space Sci., 48,* 797–799.

Jaeger J. C. and Cook N. G. W. (1969) *Fundamentals of Rock Mechanics.* Chapman and Hall, London. 515 pp.

Jaeger H. M., Nagel S. R., and Behringer R. P. (1996) The physics of granular materials. *Phys. Today, 49,* 32–39.

Jiongming S., Binglu S., and Bin W. (1998) Dynamics of size segregation of granular materials by shaking. *Nuovo Cimento, 20,* 1443.

Keil K. (2002) Geological history of asteroid 4 Vesta: The "smallest terrestrial planet." In *Asteroids III* (W. F. Bottke Jr. et al., eds.), this volume. Univ. of Arizona, Tucson.

Keil K., Haack H., and Scott E. R. D. (1994) Catastrophic fragmentation of asteroids: Evidence from meteorites. *Planet. Space Sci., 42,* 1109–1122.

Kofman W. and 20 colleagues (1998) Comet nucleus sounding experiment by radiowave transmission. *Adv. Space Res., 21,* 1589–1598.

Lange M. A. and Ahrens T. J (1983) The dynamic tensile strength of ice and ice-silicate mixtures. *J. Geophys. Res., 88,* 1197–1208.

Lawn B. R. and Wilshaw T. R. (1975) *Fracture of Brittle Solids.* Cambridge Univ., Cambridge. 160 pp.

Lee P. C. (1996) Dust levitation on asteroids. *Icarus, 124,* 181–194.

Leinhardt Z. M., Richardson D. C., and Quinn T. (2000) Direct N-body simulations of rubble pile collisions. *Icarus, 146,* 133–151.

Lindholm U. S., Yeakley L. M., and Nagy A. (1974) The dynamic strength and fracture properties of Dressler basalt. *Intl. J. Rock Mech. Min. Sci. Geomech. Abstr., 11,* 181–191.

Love S. G. and Ahrens T. J. (1996) Catastrophic impacts on grav-

ity dominated asteroids. *Icarus, 124,* 141–155.

Love S. G., Hörz F., and Brownlee D. E. (1993) Target porosity effects in impact cratering and collisional disruption. *Icarus, 105,* 216–224.

Martelli G., Ryan E. V., Nakamura A. M., and Giblin I. (1994) Catastrophic disruption experiments: Recent results. *Planet. Space Sci., 42,* 1013–1026.

McSween H. Y. (1999) *Meteorites and Their Parent Planets,* 2nd edition. Cambridge Univ., New York. 322 pp.

McSween H. Y. Jr., Ghosh A., Grimm R. E., Wilson L., and Young E. D. (2002) Thermal evolution models of asteroids. In *Asteroids III* (W. F. Bottke Jr. et al., eds.), this volume. Univ. of Arizona, Tucson.

Melosh H. J. and Ryan E. V. (1997) Asteroids: Shattered but not dispersed. *Icarus, 129,* 562–564.

Melosh H. J., Ryan E. V., and Asphaug E. (1992) Dynamic fragmentation in impacts: Hydrocode simulation of laboratory impacts. *J. Geophys. Res., 97,* 14735–14759.

Melosh H. J., Nemchinov I. V., and Zetzer Yu. I. (1994) Nonnuclear strategies for deflecting comets and asteroids. In *Hazards Due to Comets and Asteroids* (T. Gehrels, ed.), pp. 1111–1132. Univ. of Arizona, Tucson.

Merline W. J., Weidenschilling S. J., Durda D. D., Margot J.-L., Pravec P., and Storrs A. D. (2002) Asteroids *do* have satellites. In *Asteroids III* (W. F. Bottke Jr. et al., eds.), this volume. Univ. of Arizona, Tucson.

Morbidelli A., Bottke W. F. Jr., Froeschlé Ch., and Michel P. (2002) Origin and evolution of near-Earth objects. In *Asteroids III* (W. F. Bottke Jr. et al., eds.), this volume. Univ. of Arizona, Tucson.

Nolan M. C., Asphaug E., Melosh H. J., and Greenberg R. (1996) Impact craters on asteroids: Does gravity or strength control their size? *Icarus, 124,* 359–371.

Ostro S. J., Chandler J. F., Hine A. A., Rosema K. D., Shapiro I. I., and Yeomans D. K. (1990) Radar images of asteroid 1989 PB. *Science, 248,* 1523–1528.

Ostro S. J., Pravec P., Benner L. A. M., Hudson R. S., Sarounova L., Hicks M. D., Rabinowitz D. L., Scotti J. V., Tholen D. J., Wolf M., Jurgens R. F., Thomas M. L., Giorgini J. D., Chodas P. W., Yeomans D. K., Rose R., Frye R., Rosema K. D., Winkler R., and Slade M. A. (1999) Radar and optical observations of asteroid 1998 KY26. *Science, 285,* 557–559.

Ostro S. J., Hudson R. S., Benner L. A. M., Giorgini J. D., Magri C., Margot J.-L., and Nolan M. C. (2002) Asteroid radar astronomy. In *Asteroids III* (W. F. Bottke Jr. et al., eds.), this volume. Univ. of Arizona, Tucson.

Perret W. R., Rutter R. L., Millsap F. K., Thornbrough A. D., and Hansen G. H. (1967) *Free-Field Particle Motion from a Nuclear Explosion in Salt, Part I, Project Dribble, Salmon Event.* Sandia Rept. VUF-3012, Sandia Laboratory.

Pravec P. and Harris A. W. (2000) Fast and slow rotation of asteroids. *Icarus, 148,* 12–20.

Pravec P., Harris A. W., and Michałowski T. (2002) Asteroid rotations. In *Asteroids III* (W. F. Bottke Jr. et al., eds.), this volume. Univ. of Arizona, Tucson.

Prockter L., Thomas P., Robinson M., Joseph J., Milne A., Bussey B., Veverka J., and Cheng A. (2002) Surface expressions of structural features on Eros. *Icarus, 155,* 75–93.

Richardson D. C., Leinhardt Z. M., Melosh H. J., Bottke W. F. Jr., and Asphaug E. (2002) Gravitational aggregates: Evidence and evolution. In *Asteroids III* (W. F. Bottke Jr. et al., eds.), this volume. Univ. of Arizona, Tucson.

Rinehart J. S. (1965) Dynamic fracture strength of rocks. *Proc. 7th Symposium on Rock Mechanics, Vol. 1,* pp. 205–208.

Rivkin A. S., Clark B. E., Britt D. T., and Lebofsky L. A. (1997) Infrared spectrophotometry of the NEAR flyby target 253 Mathilde. *Icarus, 127,* 255–257.

Rivkin A. S., Howell E. S., Vilas F., and Lebofsky L. A. (2002) Hydrated minerals on asteroids: The astronomical record. In *Asteroids III* (W. F. Bottke Jr. et al., eds.), this volume. Univ. of Arizona, Tucson.

Rodionov V. N., Adushkin V. V., Kostyuchenko V. N., Nikolaevskii V. N., Romashov A. N., Sadovskii M. A., and Tsvetkov V. M. (1972) *Mechanical Effect of an Underground Explosion*. U.S. Atomic Energy Commission, Los Alamos.

Rubincam D. P. (2000) Radiative spin-up and spin-down of small asteroids. *Icarus, 148,* 2–11.

Ryan E. V. (1992) Catastrophic collisions: Laboratory impact experiments, hydrocode simulations, and the scaling problem. Ph.D. thesis, Univ. of Arizona, Tucson.

Ryan E. V. and Melosh H. J. (1998) Impact fragmentation: From the laboratory to asteroids. *Icarus, 133,* 1–24.

Ryan E.V., Hartmann W. K., and Davis D. R. (1991) Impact experiments III — Catastrophic fragmentation of aggregate targets and relation to asteroids. *Icarus, 94,* 283–298.

Sagdeev R. Z., Elaysberg P. E., and Moroz V. I. (1987) An estimate of the mass and density of the Comet Halley nucleus. *Pisma Astron. Zh., 13,* 621–629.

Scott E. R. D., Taylor G. J., Newsom H. E., Herbert F., and Zolensky M. (1989) Chemical, thermal and impact processing of asteroids. In *Asteroids II* (R. P. Binzel et al., eds.), pp. 701–739. Univ. of Arizona, Tucson.

Sears D. W. G. and Akridge D. G. (1998) Nebular or parent body alteration of chondritic material: Neither or both? *Meteoritics & Planet. Sci., 33,* 1157–1167.

Sekanina Z., Chodas P. W., and Yeomans D. K. (1994) Tidal disruption and the appearance of periodic comet Shoemaker-Levy 9. *Astron. Astrophys., 289,* 607–636.

Stewart S. T., Ahrens T. J., and Lange M. A. (1999) Correction to the dynamic tensile strength of ice and ice-silicate mixtures (Lange and Ahrens 1983) (abstract). In *Lunar and Planetary Science XXX,* Abstract #2037. Lunar and Planetary Institute, Houston (CD-ROM).

Sullivan R. J., Thomas P. C., Murchie S. L., and Robinson M. S. (2002) Asteroid geology from Galileo and NEAR Shoemaker data. In *Asteroids III* (W. F. Bottke Jr. et al., eds.), this volume. Univ. of Arizona, Tucson.

Thomas P. C. (1998) Ejecta emplacement on the martian satellites. *Icarus, 131,* 78–106.

Thomas P., Veverka J., Bloom A., and Duxbury T. (1979) Grooves on Phobos: Their distribution, morphology, and possible origin. *J. Geophys. Res., 84,* 8457–8477.

Thomas P. C., Belton M. J. S., Carcich B., Chapman C. R., Davies M. E., Sullivan R., and Veverka J. (1996) The shape of Ida. *Icarus, 120,* 20–32.

Thomas P. C. and 11 colleagues (1999) Mathilde: Size, shape, and geology. *Icarus, 140,* 17–27.

Thomas P. C., Veverka J., Sullivan R., Simonelli D. P., Malin M. C., Caplinger M., Hartmann W. K., and James P. B. (2000) Phobos: Regolith and ejecta blocks investigated with Mars Orbiter Camera images. *J. Geophys. Res., 105,* 15091–15106.

Thomas P. C., Veverka J., Robinson M. S., and Murchie S. (2001) Shoemaker crater as the source of most ejecta blocks on the asteroid 433 Eros. *Nature, 413,* 394–396.

Tonks W. B. and Melosh H. J. (1992) Core formation by giant impacts. *Icarus, 100,* 326–346.

Trombka, J. I. and 23 colleagues (2000) The elemental composition of asteroid 433 Eros: Results of the NEAR Shoemaker X-ray spectrometer. *Science, 289,* 2101–2105.

Trucano G. T. and Grady D. E. (1995) Impact shock and penetration fragmentation in porous media. *J. Impact Eng., 17,* 861–872.

Veverka J. and Thomas P. (1979) Phobos and Deimos — A preview of what asteroids are like? In *Asteroids* (T. Gehrels, ed.), pp. 628–651. Univ. of Arizona, Tucson.

Veverka J., Thomas P., Johnson T. V., Matson D., and Housen K. (1986) The physical characteristics of satellite surfaces. In *Satellites* (J. A. Burns and M. S. Matthews, eds.), pp. 342–402. Univ. of Arizona, Tucson.

Veverka J. and 16 colleagues (1997) NEAR's flyby of 253 Mathilde: Images of a C asteroid. *Science, 278,* 2109–2112.

von Neumann J. and Richtmyer R. D. (1950) A method for the numerical calculation of hydrodynamic shocks. *J. Appl. Phys., 21,* 232–237.

Warren P. H. (1994) Lunar and martian meteorite delivery services. *Icarus, 111,* 338–363.

Weibull W. A. (1939) A statistical theory of the strength of materials (translation). *Ingvetensk. Akad. Handl. (Stockholm), 151,* 5–45.

Weibull W. A. (1951) A statistical distribution function of wide applicability. *J. Appl. Mech., 18,* 293–297.

Weidenschilling S. J. and Cuzzi J. N. (1993) Formation of planetesimals in the solar nebula. In *Protostars and Planets III* (E. H. Levy and J. I. Lunine, eds.), pp. 1031–1060. Univ. of Arizona, Tucson.

Weissman P. R. (1986) Are cometary nuclei primordial rubble piles? *Nature, 320,* 242–244.

Weissman P. R., Bottke W. F. Jr., and Levison H. F. (2002) Evolution of comets into asteroids. In *Asteroids III* (W. F. Bottke Jr. et al., eds.), this volume. Univ. of Arizona, Tucson.

Wetherill G. W. (1985) Occurrence of giant impacts during the growth of the terrestrial planets. *Science, 228,* 877–879.

Whipple F. L. (1949) Comets, meteors and the interplanetary complex. *Astron. J., 54,* 179–180.

Wu R. and Yang F. (1997) Seismic imaging in wavelet domain: Decomposition and compression of imaging operator. In *Wavelet Applications in Signal and Image Processing* (V. A. Aldroubi et al., eds.), pp. 148–162. Proc. SPIE Vol. 3169.

Yeomans D. K. and 15 colleagues (2000) Radio science results during the NEAR Shoemaker spacecraft rendezvous with Eros. *Science, 289,* 2085–2088.

Zappalà V., Cellino A., Dell'Oro A., and Paolicchi P. (2002) Physical and dynamical properties of asteroid families. In *Asteroids III* (W. F. Bottke Jr. et al., eds.), this volume. Univ. of Arizona, Tucson.

Zuber M. T. and 11 colleagues (2000) The shape of 433 Eros from the NEAR Shoemaker Laser Rangefinder. *Science, 289,* 2097–2101.